The mitochondrial translocase of the inner membrane PaTim54 is involved in defense response and longevity in Podospora anserina

Alex Mercier, Colin Clairet, Robert Debuchy, David Morais, Philippe Silar, Sylvain Brun

The Mitochondrial Translocase of the Inner Membrane PaTim54 is involved in Defense Response and Longevity in *Podospora anserina*

Alex Mercier[1#], Colin Clairet[1#], Robert Debuchy[2#], David Morais[1], Philippe Silar[1] and Sylvain Brun[1*]

1: Univ. Paris-Diderot, LIED-Laboratoire Interdisciplinaire des Energies de Demain-UMR 82365, 5 rue Marie-Andree Lagroua-Weill-Hall, 75205 Paris cedex, France

2: Institute for Integrative Biology of the Cell (I2BC), CEA, CNRS, Univ. Paris-Sud, Universite Paris-Saclay, 91198, Gif-sur-Yvette cedex, France

Alex Mercier and Colin Clairet present address: INRA UMR 1290 Bioger, 1 Avenue Lucien Bretignières, 78850 Thiverval-Grignon, France

#: Alex Mercier, Colin Clairet and Robert Debuchy should be considered joint first authors

*: **Correspondance to Dr. Sylvain Brun:** sylvain.brun@univ-paris-diderot.fr ; tel: 00 33 1 57 27 84 73

Key words: Tim54, Hyphal Interference, aging, mitochondria, *Podospora anserina*, fungi

Running title: *PaTim54* controls Defense Response and Longevity in *P. anserina*

Abstract

Fungi are very successful microorganisms capable of colonizing virtually any ecological niche where they must constantly cope with competitors including fungi, bacteria and nematodes. We have shown previously that the ascomycete *Podopora anserina* exhibits Hyphal Interference (HI), an antagonistic response triggered by direct contact of competing fungal hyphae. When challenged with *Penicillium chrysogenum*, *P. anserina* produces hydrogen peroxide at the confrontation and kills the hyphae of *P. chrysogenum*. Here, we report the characterization of the *PDC*^{2218} mutant affected in HI. When challenged with *P. chrysogenum*, the *PDC*^{2218} mutant produces a massive oxidative burst at the confrontation. However, this increased production of hydrogen peroxide is not correlated to increased cell death in *P. chrysogenum*. Hence, the oxidative burst and cell death in the challenger are uncoupled in *PDC*^{2218}. The gene affected in *PDC*^{2218} is *PaTim54,* encoding the homologue of the budding yeast mitochondrial inner membrane import machinery component Tim54p. We show that *PaTim54* is essential in *P. anserina* and that the phenotypes displayed by the *PDC*^{2218} mutant, renamed *PaTim54*^{2218}, are the consequence of a drastic reduction in the expression of *PaTim54*. Among these pleiotropic phenotypes, *PDC*^{2218}*-PaTim54*^{2218}- displays increased lifespan, a phenotype in line with the observed mitochondrial defects in the mutant.

1. Introduction

Fungi are very successful microorganisms capable of colonizing virtually any ecological niche where they must constantly cope with competitors such as other fungi, bacteria, nematodes (Boddy, 2000; Boddy and Hiscox, 2016; Crowther et al., 2012). Fungi are often engaged in multiple kinds of biotic interactions ranging from symbiotic to antagonistic (DeVay, 1956). In particular, saprotrophic fungi that compete for nutrients have developed strategies to avoid spreading of competitors. Antibiosis, the most famous and the most studied antagonistic interaction is viewed as a long-distance process that mainly relies on the capacity of fungi to constitutively produce and secrete toxic secondary metabolites (Macheleidt et al., 2016). Hyphal interference (HI) and mycoparasitism are on the contrary responses engaged after direct contact with challengers. Triggering such antagonistic interactions implies that fungi must be endowed with a non-self-recognition system to adapt the nature of the interaction with the competitor (Silar, 2012; Uehling et al., 2017). Non-self-recognition has been studied in Vegetative Incompatibility (VI) observed in both ascomycete model systems *Neurospora crassa* and *Podospora anserina* but this phenomenon involves competitors from the same species (Glass et al., 2000; Saupe et al., 2000). On the contrary, HI (and mycoparasitism) takes place between competitors from different species. HI was first investigated by Ikediugwu and Websters who demonstrated that the basidiomycete *Coprinus heptemerus* kills hyphal cells of several ascomycetes competitors at the confrontation between thalli (Ikediugwu, 1976; Ikediugwu et al., 1970; Ikediugwu and Webster, 1970). Although in both VI and HI, the eventual outcome is the death of fungal cells, the major discrepancy between VI and HI is the oxidative burst observed in HI only (Silar, 2005). Indeed, when *P. anserina* is challenged by *Penicillium chrysogenum*, hydrogen peroxide accumulates on the thallus of *P. anserina* at the confrontation and it has been shown that cells of *P. chrysogenum* in contact with those of *P. anserina* are killed. This latter feature of HI resembles the oxidative burst taking place during innate immune response that kills or limit the spreading of invading pathogens in both plants and animals (Iles and Forman, 2002; Liu and He, 2016; Marino et al., 2012). This analogy with the innate immune response of higher Eukaryotes was further

strengthened when it was shown in *P. anserina* that HI requires the NADPH oxidase (Nox) PaNox1, the homologue of mammalian NOX2/gp91^{phox} and of plant Rboh O_2^--producing enzymes (Silar, 2005). Indeed, when the *PaNox1*$^-$ mutant is challenged with *P. chrysogenum*, the accumulation of hydrogen peroxide on the mutant thallus on the one hand and cell death in *P. chrysogenum* on the other hand are decreased at the confrontation of both mycelia. Noteworthy, three Nox isoforms are found in fungi, Nox1/A, Nox2/B and Nox3/C. While the role of Nox3/C remains unknown, *Nox1/A* and/or *Nox2/B* regulate an astonishing number of processes such as cellulose degradation, anastomosis (cell fusion), sexual reproduction, ascospore germination, cytoskeleton remodeling, symbiosis and pathogeny (Aguirre et al., 2005; Brun et al., 2009; Scott, 2015; Scott and Eaton, 2008; Tudzynski et al., 2012). However, only PaNox1 regulates HI (Brun et al., 2009; Silar, 2005).

In *P. anserina*, *IDC*^{343}, the mutant of *PaNox1* was isolated in a screen designed to identify mutants of Crippled Growth (CG), an epigenetically triggered mycelial degeneration observed when *P. anserina* is grown on specific media (Haedens et al., 2005; Silar et al., 1999). Several *Impaired Development of CG* (*IDC*) mutants proved to be pleiotropic mutants defective in processes such as HI. In particular, mutants of the PaNox1 complex or of the Cell Wall Integrity pathway (CWI) PaMpk1 MAP Kinase pathway, are *IDC* mutants that exert similar HI defects as *PaNox1* (Brun et al., 2009; Lacaze et al., 2015; Silar, 2005). Not only *IDC* mutants have been isolated in the original screens for CG mutants: *Promote Development of CG* (*PDC*) mutants were also isolated and tested for HI. Amongst these *IDC* and *PDC* mutants, the *PDC*^{2218} mutant showed unusual phenotype for HI. When challenged with *P. chrysogenum*, the *PDC*^{2218} mutant produces a massive oxidative burst at the confrontation. However, this increased production of hydrogen peroxide by the *PDC*^{2218} mutant is not correlated to increased cell death in *P. chrysogenum* (Silar, 2012). In this mutant, recognition of *P. chrysogenum* likely occurs but the triggered response appears abnormal. Especially, the oxidative burst and cell death in the challenger are uncoupled, which strengthen the previous assumption that hydrogen peroxide has a signaling role rather than a toxic one (Brun et al., 2009; Silar, 2005). With the aim to get insights into the link between the oxidative burst in *P. anserina* and HI-induced cell death in the challenger, the

identification of the gene affected in *PDC*^{2218} was undertaken. We first proceeded to positional cloning of the mutation and we identified a deletion spanning 1560 bp in the mutant genome. Even though the deletion disrupts the 5' part of the *PaNip30* putative CDS as well as part of the 3' UTR (UnTranslated Region) of the neighboring *PaCdk5* putative gene, our investigations show that none of these genes are important for HI. Indeed, by a combination of different approaches: functional complementation, gene deletion, genetic analyses and gene expression data, we show here that the gene important for creating the HI phenotype in *PDC*^{2218} is *PaTim54*, the gene encoding the homologue of the budding yeast mitochondria inner membrane carrier Tim54p (Hwang et al., 2007; Kerscher et al., 1997; Kurz et al., 1999). Surprisingly, this gene is located more than 1000 bp away from the deletion. We show that *PaTim54* is essential in *P. anserina* and that the phenotypes displayed by the hypomorphic *PDC*^{2218} mutant (renamed *PaTim54*^{2218}) are the consequence of a drastic reduction in the expression of *PaTim54*.

Contrary to many filamentous fungi, *P. anserina* has a limited vegetative growth phase that terminates by a the senescence of the cells at the thallus apex (Rizet, 1953a). For decades, this fungus has been a successful model system in studying aging and especially the effects of mitochondrial disorders in this degenerative process (Lorin et al., 2006; Osiewacz et al., 2010). In this paper, we show that the *PaTim54*^{2218} mutation increases longevity and alters the respiratory chain, mitochondrial DNA (mtDNA) nucleoids as well as mitochondria morphology.

2. Materials and methods

2.1. Strains, culture conditions and DNA preparations

All the strains used in this study (Table 1) derived from the "S" (big S) wild-type strain that was used for sequencing the *P. anserina* genome (Espagne et al., 2008). The genome sequence and EST derived from the S strain are available at http://podospora.i2bc.paris-saclay.fr/. The polymorphic *P. comata* strain T was used for positional cloning of the *PDC*^{2218} mutation (Boucher et al., 2017). The *PDC*^{2218} (*PaTim54*^{2218}) and the *PaNox1*$^{-}$ (*IDC*^{343}) strains were first described in (Haedens et al., 2005); the

ΔPaMpk1 in (Kicka et al., 2006) and the *mito-GFP* strain in (Sellem et al., 2007). All the deletions by homologous recombination have been performed in strains inactivated for *Pamus51*, the gene encoding the helicase of the NHEJ repair system, enhancing homologous recombination in these strains (El-Khoury et al., 2008). Standard culture conditions, media and genetic methods for *P. anserina* are reported in http://podospora.i2bc.paris-saclay.fr/; the M2 standard medium is a medium in which carbon is supplied as dextrin, and nitrogen as urea. The methods used for nucleic acid extraction and manipulation have been described (Lecellier and Silar, 1994). Transformation of *P. anserina* protoplasts was carried out as described previously (Debuchy and Brygoo, 1985).

2.2. Deletion of *PaCdk5*

The *PaCdk5 (Pa_6__9000)* predicted CDS was deleted by a split-marker strategy (Lalucque et al., 2012). To construct the deletion cassette of the entire *PaCdk5* coding sequence, a hygromycin B resistance (hygR) marker was fused by PCR with the upstream or the downstream sequence of the *PaCdk5* gene (Fig. S1). 1063 bp upstream and 1009 bp downstream of *PaCdk5* were amplified from the wild-type genomic DNA with primers 9000_1 and 9000_2 for the upstream region and 9000_10 and 9000_11 for the downstream region (Table S1). Primers 9000_2 and 9000_10 contained additional bases allowing fusion with the hygR cassette. The hygR cassette was amplified using primers 9000_HYGF/9000_HYGR with pBC-hyg plasmid as template (Silar, 1995). In a second step, two amplification reactions were performed using primers 9000_1/HY and YG/9000_11 to obtain the fusion of two PCR products, the upstream (5') region/hygR and hygR/downstream (3') region. The mixture of these two PCR products was used to transform a *Δmus51::phleoR* strain (El-Khoury et al., 2008) All the transformants showed a similar mutant phenotype (Figure 1). For twelve of them, integration of the deletion K7 was checked by PCR using primers 9000_5/HygL for the 5' flanking sequences and HygR/214-6bis for the 3' flanking sequences. One *Δmus51::phleoR ΔPaCdk5::hygR* transformant was crossed with the wild type and homokaryotic [phleoS hygR] *ΔPaCdk5::hygR* progeny was selected for further studies and analyzed by Southern blotting to confirm deletion of *PaCdk5* (Figure S1).

2.3. Deletion of *PaNip30*

The *PaNip30 (Pa_6_9010)* predicted CDS was deleted by a PCR-based strategy (Lalucque et al., 2012). To construct the deletion cassette of the entire *PaNip30* coding sequence, a nourseothricin resistance (nouR) marker was fused by PCR with the upstream or the downstream sequence of the *PaNip30* gene (Figure S1). 514 bp upstream and 484 bp downstream of *PaNip30* were amplified from wild-type genomic DNA with primers 9010_1 and 9010_2 for the upstream region and primers 9010_5 and 9010_6 for the downstream region (Table S1). Primers 9010_2 and 9010_5 contained additional bases allowing fusion with the nouR cassette. The nouR cassette was amplified using primers 9010_MKF/9010_MKR from pBC-nour plasmid (Lalucque et al., 2012). In a second step, two amplification reactions were performed using 9010_1/9010_MKR and 9010_MKF /9010_6 primers pairs to obtain the fusion of two PCR products, the upstream (5') region/nouR and nouR/downstream (3') region. The mixture of these two PCR products was used to transform a *Δmus51::phleoR* strain (El-Khoury et al., 2008). All the transformants exerted a wild-type phenotype (Figure 1). For twelve of them, integration of the deletion K7 was checked by PCR using primers 9000_10/validMK5' for the 5' flanking sequences and validMK3'/10_20_2R for the 3' flanking sequences. One *Δmus51::phleoR ΔPaNip30::nouR* transformant was crossed with the wild type and homokaryotic [phleoS nouR] *ΔPaNip30::nouR* progeny was selected for further studies and analyz

ed by Southern blotting to confirm deletion of *PaNip30* (Figure S1).

2.4. Double deletion of *PaCdk5* and *PaNip30*

The 5' hygR and 3'hyR split-marker deletion cassettes designed to target *PaCdk5* (described above) have been introduced into a purified [phleoR nouR] *Δmus51::phleoR ΔPaNip30::nouR* homokaryotic strain by transformation. All The [hygR] transformants exerted a [*ΔPaCdk5*] mutant phenotype (Figure 1). Six transformants were selected and integration of the hygR cassette was checked by PCR using primers 9000_5/HygL for the 5' flanking sequences and HygR/validMK5' for the whole intergenic region in between *PaCdk5* and *PaNip30* deleted CDS as the HygR primer hybridises in the

hygR deletion cassette of *ΔPaCdk5::hygR* and validMK5' hybridises in the nouR deletion cassette of *ΔPaNip30::nouR*. Three *Δmus51::phleoR ΔPaCdk5::hygR ΔPaNip30::nouR* transformants were crossed with the wild type and homokaryotic [phleoS hygR nouR] progeny were selected for further studies. Proper deletion of both genes was verified by Southern blotting (Figure S1) and the PCR product corresponding to the amplification of the intergenic region (using primers HygR/validMK5') was sequenced, further confirming the integrity of the intergenic space (data not shown).

2.5. Deletion of *PaTim54*

The *PaTim54 (Pa_6__9020)* predicted CDS was deleted by a split-marker strategy (Lalucque et al., 2012). To construct the deletion cassette of the entire *PaTim54* coding sequence, a hygromycin B resistance (hygR) marker was fused by PCR with the upstream or the downstream sequence of the *PaTim54* gene (Figure S1). 1102 bp upstream and 832 bp downstream of *PaTim54* were amplified from the wild-type genomic DNA with primers 9020_3 and 9020_4 for the upstream region and 9020_1 and 9000_2 for the downstream region (Table S1). Primers 9020_2 and 9020_3 contained additional bases allowing fusion with the hygR cassette. The hygR cassette was amplified using primers 9020_HYGF/9020_HYGR from pBC-hyg plasmid as previously described. In a second step, two amplification reactions were performed using primers 9020_1/HY and YG/9020_4 to obtain the fusion of two PCR products, the upstream (5') region/hygR and hygR/downstream (3') region. The mixture of these two PCR products was used to transform a *Δmus51::su8-1* strain (El-Khoury et al., 2008, p.). All the transformants exerted wild-type phenotype (data not shown). For twelve of them, integration of the deletion K7 was checked by PCR using primers HyGR/9020_5 for the 5' flanking sequences and 9010_2F/HygL for the 3' flanking sequences. Two *Δmus51::su8-1 ΔPaTim54::hygR* transformants bearing PCR-verified hygR deletion cassette were crossed with the wild type. However, no homokaryotic [hygR] progeny was obtained. Further evidences argued that these two primary transformants were heterokaryotic and that deletion of *PaTim54* is lethal (see results).

2.6. Plasmids

The pBC-hyg and pBC-phleo have been described in (Silar, 1995). Cosmids of the *P. anserina* genomic library ref: 27C11, 31C04, 8H08, 11G02, 46G03, 1B05, 44C04, 3H09, 8C03, 38F08, 36C09, 39C12 and 12F01 bearing an hygR selection marker have been used for positional cloning. Plasmids of the *P. anserina* genomic library ref: 342AG09 (bearing the *Pa_6_8980* CDS), 340DH08 (*Pa_6_8990* CDS), 224BE12 (*Pa_6_8991* CDS), 328CD12 (*Pa_6_9000* CDS) renamed pPaCdk5, 193BG01 (*Pa_6_9010* CDS) renamed pPaNip30, 434CF12 (*Pa_6_9020* CDS) renamed pPaTim54 and 142DC07 (*Pa_6_9030* CDS) have been used for positional cloning. The pCDNA.2 plasmid backbone does not bear selection marker in *P. anserina*. The average size of the insert is 3 kbp (Espagne et al., 2008).

2.7. Constructions

2.7.1. pBC-hyg-PaCdk5: The pPaCdk5 plasmid was digested by the *Not*I and *Spe*I restriction enzymes. It generated a 3632 bp fragment bearing the 1023 bp of *PaCdk5* predicted CDS plus the 1536 bp upstream and the 1073 bp downstream of *PaCdk5* predicted CDS. This insert was subcloned into *Not*1/*Spe*I-digested pBC-hyg generating the pBC-hyg-PaCdk5 plasmid.

2.7.2. pBC-hyg-PaTim54 and pBC-phleo-PaTim54: The pPaTim54 plasmid was digested by the *Spe*I and *Xho*I restriction enzymes. It generated a 3135 bp fragment bearing a 1450 bp encompassing *pPaTim54* predicted CDS (1386 bp) and one intron (64 bp) plus the 1019 bp upstream and the 666 bp downstream of *PaTim54* predicted CDS. This insert was subcloned into *Spe*I/*Xho*I-digested pBC-hyg or pBC-phleo, generating the pBC-hyg-PaTim54 and the pBC-phleo-PaTim54 plasmids respectively.

2.8. PCR based complementation of *PaTim54^{2218}*: The *PaCdk5^{PCR}* PCR fragment encompassing the 152 base pairs upstream of the *PaCdk5* CDS as well as the 139 base pairs downstream of the CDS was generated from wild-type genomic DNA using primers 9000_1F/9000_4R (Table S1) (GoTaq, Promega). The *PaTim54^{PCR}* PCR fragment encompassing the 504 base pairs upstream of *PaTim54* CDS, the *PaTim54* CDS as well as the 182 base pairs downstream of the CDS was generated from wild-type genomic DNA using primers 9020_6F/9020_5R (Table S1). Each PCR fragment was co-transformed with pBC-hyg into *PaTim54^{2218}* with a 3:1.

212 **2.9. RNA isolation and RT-qPCR**

213 Vegetative cultures for RNA preparation were performed on Petri dishes containing standard M2
214 minimal medium and covered with a cellophane sheet. These cultures were inoculated with 6
215 implants from *mat* - wild-type strain or mutants. Dishes were placed at 27°C under standard light and
216 were removed from the incubation room at 48 h. Biological materials were collected and flash-frozen
217 in liquid nitrogen. Total RNA of *P. anserina* was extracted using the RNeasy Plant Mini Kit (cat#74904,
218 Qiagen, Hilden, Germany), including a grinding process using a tissue lyser II (QIAGEN) and a DNase
219 treatment on column. The total RNA quality was checked on gel after standard electrophoresis and
220 quantity was determined by using a Nanodrop spectrophotometer (Nanodrop Technologies). 4 µg of
221 total RNA was used for the RT; reverse transcription was performed with Superscript III or RevertAid
222 (Thermo Fisher Scientific). The 9000RTF and 9000RTR primers for the qPCR on *Pa_6_9000/PaCdk5*
223 are located within the CDS at position +723 and +922 respectively. The 9020RTF and 9020RTR
224 primers for the qPCR on Pa_6_9020/PaTim54 are located at position +62 (overlapping the single
225 encoded intron) and position +359 respectively. To quantify the genes with introns, all primers were
226 designed against two consecutive exons (Table S5), and an NRT (Not Reverse Transcribed) control
227 was performed on a pool of replicates to ensure that the Cq was above the Cq obtained from
228 corresponding reverse transcribed RNAs. Each RT-qPCR experiment contained at least three
229 biological replicates (n = 6 for the $PaTim54^{2218}$ mutant) (Table S6 and S7), and each biological
230 replicate was analyzed with three technical triplicates. Normalization genes were selected from a
231 pool of 7 housekeeping genes using geNorm (Table S6) (Vandesompele et al., 2002). RT-qPCR
232 normalization according to the ΔΔCq method (Pfaffl et al., 2002), standard error and 95% confidence
233 interval calculations, and statistical analyses were performed using REST 2009 software (Qiagen,
234 Hilden, Germany). Table S8 shows fold-changes and standard errors. Genes were defined as
235 downregulated in the mutant strain if the ratio of their transcript level in the mutant strain compared
236 with that in the wild-type strain showed a fold change > 0 and < 1 and with a p-value of < 0.05. On
237 the other hand, genes were defined as up-regulated in the mutant strain if the ratio of their

transcript level in the mutant strain compared with that in the wild-type strain showed a > 1 fold change and with a p-value < 0.05. Ratios with a 95 % confidence interval, including 1, were not considered significant (du Prel et al., 2009).

2.10. DNA isolation and qPCR for mtDNA quantification

DNA was prepared as mentioned before (Lecellier and Silar, 1994). An additionnal RNAse step was added requiring a second phenol-chloroform extraction step before final DNA precipitation. For the senDNA assay (Figure 7B), DNA from the senescent apex of a *WT* strain grown 15 days on M2 medium was extracted. The mitochondrial DNA was quantified with primers targeted to *NAD4* gene and normalized to three nuclear loci corresponding to genes *PaHMG8*, *PaHMG9* and *MFM.* Importantly, *NAD4* was chosen as the target because its chromosomal location is away from the main chromosomal rearrangement leading to senDNA (Cummings et al., 1990). Each qPCR experiment contained four biological replicates and each biological replicate was analyzed with three technical replicates. The mitochondrial copy number normalization was performed according to the ΔΔCq method (Pfaffl et al., 2002) by using nuclear loci normalization genes. Standard error and 95% confidence interval calculations, and statistical analyses were performed using REST 2009 software (Qiagen, Hilden, Germany) (Pfaffl et al., 2002). Table S10 shows fold-changes and standard errors.

2.11. Microscopic analyses

Microscopic observations were made on 3 to 5 days old mycelia grown directly on agar. One cm^2 agar plugs were deposited onto a coverslip and mounted in water supplemented with DAPI (4',6-Diamidine-2'-phenylindole dihydrochloride ; Sigma-Aldrich) 0.1 $\mu g.mL^{-1}$. For pictures of confrontation between *P. anserina* and *P. chrysogenum*, plates were co-inoculated, incubated 3 days at 27°C and agar plugs at the confrontation between both species were cut and mounted as previously described but in water. Pictures were taken with an inverted microscope Leica DMI6000; sCMOS camera; LED EL6000 ; dichroic filters XF131 (DAPI) and Qmaxgreen (GFP); Imagoseine Imaging Facility: https://imagoseine.ijm.fr/676/accueil.htm . Pictures were analyzed with Fiji (Schindelin et al., 2012).

Diameter of nucleoids and of mitochondria was manually determined on undeconvoluted 2D images using the Fiji software. The size (diameter) of 20 nucleoids (n=20) and the diameter of 20 mitochondria (n=20) has been determined on two to five representative fields of view (pictures) depending on the genotype analyzed. Indeed, since the number of nucleoids and of mitochondria was lower in the *+, mito-GFP* and the *PaTim54^{2218} pBC-phleo-PaTim54 mito-GFP* strains than in the *PaTim54^{2218} mito-GFP* strain, more samples (pictures) were required to count the 20 nucleoids and the 20 mitochondria in both former strains. **GFP fluorescence intensities** in the *mito-GFP* control strain and in the Pa*Tim54^{2218} mito-GFP* strain were determined using the Fiji software as followed: The maximum fluorescence intensity for five different transversal cuts along hyphae in teen different samples (pictures) was measured using the "plot profile" function of the Fiji software. For every measure, the background fluorescence intensity was subtracted. The different samples were illuminated in the same conditions with the same exposure time. A t-test on the global distributions (n=50) was performed.

2.12. Hyphal Interference assay

Hyphal Interference assays were performed as described in (Silar, 2005) and adapted from (Munkres, 1990). Plates were incubated in parallel and in duplicate 3 days at 27°C on standard M2 medium. *P. anserina* and *P. chrysogenum* were co-inoculated at an approximate distance of 1.2 cm. For both DAB (diaminobenzidine, Sigma Aldrich) as well as Blue Evans (Sigma Aldrich) staining procedures, the solution was spread with a glass rod to ensure homogenous staining of thalli. For **DAB staining** (peroxide detection), plates were flooded in 100mM potassium phosphate buffer pH 6.9, 0.9 g.L^{-1} DAB and incubated 30 min at 27°C. The DAB staining solution was then discarded and pictures were taken 3-6h later. For Blue Evans staining (cell death assay), plates were flooded in 0.1% Evans Blue in water, incubated for 10 min and extensively rinsed with distilled water before pictures were taken.

2.13. Longevity assay

For each analyzed genotype, triplicate cultures from three different freshly germinated homokaryotic ascospores of each mating type were incubated on standard M2 medium in longevity tubes (30 cm long) at 27°C. These ascospores were obtained from crossings of the wild type S strain with itself, with *PaTim54*^{2218} and with *PaTim54*^{2218} *pBC-phleo-PaTim54.* To minimize inheritance of the senescence factor, the wild type S strain was used as female. For this purpose, the "male" implants were removed from the crossings plates before ascospores projections. Total growth distance after 191 days incubation was measured. t-test statistical analysis was performed to compare the growth distance mean of every tested genotypes. Note that measurements of *mat*- and *mat*+ strains of each genotype were pooled together for t-test analysis making a pool of 18 measures per genotype.

2.14. Mycelium fragmentation

A small plug of mycelium grown on agar plate is grinded is 500 µL sterile water in a FastPrep (500 rpm; 20 sec). The mixture is poured on an agar plate and individual hyphae are harvested under binocular and transferred on standard M2 medium. Homokaryosis is determined by testing the mating type of the regenerated thalli.

2.15 Senescent DNA (senDNA) assay

The senDNA assay was performed on the DNA samples used for the qPCR-based mtDNA quantification. DNA from the following genotypes: *WT*, *PaTim54*^{2218} and *PaTim54*^{2218} *pBC-phleo-PaTim54* (two of the four DNA replicates of each genotype were analyzed) as well as DNA sample from an aged *WT* culture were digested by *H*aeIII, ran on a 0.8% agarose gel and stained with Ethidium Bromide. SenDNA appear on the gel as intense and discrete bands in aged cultures only (Lorin et al., 2001). Molecular Weight marker: ThermoFisher scientific Generuler^{TM} 1 Kb DNA ladder.

3. Results

3.1. The *PDC*^{2218} mutant

311 The *PDC*^{2218} strain (all the strains used and generated in this study are reported Table 1) was isolated
312 in a screen designed to identify mutants of Crippled Growth (CG), an epigenetically-regulated
313 degeneration observed when *P. anserina* is grown on specific media (Haedens et al., 2005). The
314 "*Promote Development of Crippled Growth*" *PDC*^{2218} was isolated as a "weak" *PDC* mutant because
315 the severity of the degeneration observed on M2 standard medium was moderate. Additionally,
316 reversion of the degeneration was not clear (Haedens et al., 2005). Compared to the wild type, when
317 grown on M2 standard medium at 27°C, the *PDC*^{2218} mutant grew slower, exhibited a darker green
318 pigmentation and was almost devoid of aerial hyphae (Figure 1 and 2). This vegetative phenotype
319 allowed us to characterize the *PDC*^{2218} mutation during positional cloning of the mutation. In
320 addition, *PDC*^{2218} showed temperature sensitivity. The mutant grew much slower than the wild type
321 at 18°C and did not grow at all at 37°C (Figure 2B).

322 We have previously shown that when *P. anserina* was challenged with *P. chrysogenum*, the Hyphal
323 Interference outcome is an oxidative burst on the thallus of *P. anserina* at the confrontation
324 (revealed by DAB staining) as well as cell death in *Penicillium chrysogenum* (revealed by Trypan blue
325 or Evans blue staining) (Silar, 2005). Remarkably, the *PDC*^{2218} mutant exhibited a modified Hyphal
326 Interference (HI) when confronted with *P. chrysogenum* with higher DAB precipitation and decreased
327 Evans blue staining (Figure 1) (Silar, 2012). Hence, in the mutant, a huge oxidative burst was
328 triggered during HI but this was not correlated to increased cell death in the competitor (*i.e.*, *P.*
329 *chrysogenum*). On the contrary, *P. chrysogenum* cell death was reduced.

330 **3.2. Positional cloning of the *PDC*^{2218} mutation**

331 Previous studies determined that the *PDC*^{2218} mutation had a Second Division Segregation (SDS)
332 frequency of 85%, indicating that it was located in the distal region of the arm of one of the seven
333 chromosomes of *P. anserina* (Haedens et al., 2005). By crossing the *PDC*^{2218} mutant with different
334 strains bearing mutations in distal parts of chromosomes, we did find a genetic linkage (d=7 cM)
335 between the *PDC*^{2218} mutation and the *ΔPaTrx2* deletion (Malagnac et al., 2007) (Table S2). In

agreement with the 85% SDS of the *PaTrx2* gene, this result indicated that the *PDC*^{2218} mutation was located close to *PaTrx2* on the left arm distal part of chromosome six. Note that we finally localized the *PDC*^{2218} mutation about 93 kbp from the *PaTrx2* gene (Figure 3) (see below). We continued positional cloning of the mutation by crossing the *PDC*^{2218} mutant (generated in the big S strain) with the highly polymorphic strain T of the *Podospora comata* species (Boucher et al., 2017). We then analyzed co-segregation of polymorphic genetic markers and the *PDC*^{2218} mutation in the progeny. This allowed us to narrow down the location of the *PDC*^{2218} mutation to a 370,822 bp interval delimited by the 214-1 and Yeti-1 molecular markers (Figure 3). Thirteen cosmids of the *P. anserina* genome bank (Espagne et al., 2008) bearing wild-type sequences as well as the hygromycin B resistance gene and overlapping the candidate interval were transformed into the *PDC*^{2218} mutant (see materials and methods). Only transformation with the 11G02 cosmid gave 12 "wild-type-looking" [WT] (from now on, phenotypes are indicated in square brackets) out of 34 [hygR] transformants, suggesting that 11G02 carried the wild-type allele of the gene mutated in *PDC*^{2218}. It also indicated that the *PDC*^{2218} mutation was recessive. The 22 non-complementing transformants likely resulted from the heterologous integration of the cosmid and fortuitous inactivation of the complementing sequence. Transformation with the partially overlapping 31C04 cosmid did not provide any complemented transformant. This led us to conclude that the *PDC*^{2218} mutation was in the non-overlapping part of the sequence carried by the 11G02 cosmid, allowing us to narrow down the candidate interval for the mutation (Figure 3).

Seven predicted CDS were encoded in this interval. We selected seven plasmids of the *P. anserina* genome bank corresponding to the seven genes, each plasmid bearing a single predicted CDS (see materials and methods). Since the pCDNA.2 backbone of the bank's plasmids has no fungal selective marker, co-transformation of each plasmid along with empty pBC-hyg plasmid conferring resistance to hygromycin B was performed. Complementation of the mutant phenotype was observed both when wild-type *Pa_6_9000* (pPaCdk5 plasmid) or *Pa_6_9020* CDS (pPaTim54 plasmid) were introduced into *PDC*^{2218} (Figure 3). The *Pa_6_9000* predicted CDS encodes Pho85/PaCdk5, the *P.*

anserina homologue of the yeast Cyclin Dependent Kinase 5 (Huang et al., 2007) and *Pa_6_9020* encodes the homologue of the yeast mitochondrial Translocase of the Inner Membrane protein Tim54p, PaTim54 (Figure S2) (Kerscher et al., 1997). A total of 15 [WT] out of 137 [hygR] transformants were obtained with the plasmid carrying *PaCdk5* and 44 [WT] out of 49 [hygR] transformants were obtained with the plasmid carrying *PaTim54*. On the contrary, co-transformation with the five other selected plasmids or empty pBC-hyg plasmid alone did not promote recovery of [WT] transformants. Noteworthy, co-transformation with the plasmid bearing the predicted *PaNip30* CDS (*Pa_6_9010*), encoding the Nip30 homologue protein of unknown function (Mammalian Gene Collection (MGC) Program Team, 2002), located between *PaCdk5* and *PaTim54* on the chromosome did not result in any complementation (0 [WT]/ 35 [hygR]). These results were confirmed by co-transformation experiments performed using PCR fragments consisting of *PaCdk5* wild-type CDS (*PaCdk5*^{PCR}) or of *PaTim54's* one (*PaTim54*^{PCR}) with pBC-hyg: 4 [WT] out of 50 [hygR] transformants for *PaCdk5*^{PCR} and 88 [WT] out of 97 [hygR] transformants for *PaTim54*^{PCR} were observed (see materials and methods and Figure 3). With the aim to rule out any artefactual effect due to co-transformation, we generated the pBC-hyg-PaCdk5 and pBC-hyg-PaTim54 plasmids by cloning the *PaCdk5* and the *PaTim54* predicted CDS from pPaCdk5 and pPaTim54 into pBC-hyg respectively (see materials and methods and Figure 3). In agreement with the previous experiments, complementation of *PDC*^{2218} was observed with both pBC-hyg-PaCdk5 (15 [WT]/ 50 [hygR]) and pBC-hyg-PaTim54 (47 [WT]/ 50 [hygR]).

For the sake of simplicity, the *PDC*^{2218} mutation was renamed *PaTim54*^{2218} in the following parts of the manuscript as *PaTim54* proved to be the gene affected in *PDC*^{2218} (see below). Five *PaTim54*^{2218} *pBC-hyg-Cdk5* as well as five *PaTim54*^{2218} *pBC-hyg-PaTim54* independent transformants presenting wild-type vegetative growth were tested for HI. Every transformants showed wild-type HI indicating that the HI default was complemented as well. Representative result for one of the [WT] transformants tested is shown Figure 1. This transformant of the *PaTim54*^{2218} *pBC-hyg-Cdk5* genotype was annotated "*cis*" (see below for further explanations). Unexpectedly, taken together,

these above complementation experiments did not allow us to determine which of *PaCdk5* or *PaTim54* was affected in the *PaTim54*^{2218} mutant.

3.3. Molecular characterization of the *PaTim54*^{2218} mutation

Both *PaCdk5* and *PaTim54* genes were amplified by PCR in *PaTim54*^{2218} and sequenced. In addition to the CDS *per se*, sequencing included 458 bp upstream and 139 bp downstream of *PaCdk5* CDS as well as 372 bp upstream and 223 bp downstream of *PaTim54* CDS. Surprisingly, sequencing of both genes did not reveal any mutation. With the aim to further investigate the sequence of the region between *PaCdk5* and *PaTim54*, we attempted PCR-based chromosome walking within the 3157 bp separating both CDS (Figure 3). Strikingly, PCR amplification of the region between *PaCdk5* and *PaNip30* (using primers 9000_3F/9010_3R binding in each CDS respectively) was about 1600 bp shorter than expected in the *PaTim54*^{2218} mutant, strongly suggesting a deletion in the mutant's genome. Sequencing of this PCR product confirmed that 1560 bp were lacking in *PaTim54*^{2218}. This deletion removed the first 140 bp of *PaNip30* CDS as well as 1420 out of the 1856 bp of the intergenic region between *PaCdk5* and *PaNip30*. Analysis of *P. anserina* ESTs (Espagne et al., 2008) showed that the *PaCdk5* gene is transcribed and that it bears a long 3' UTR overlapping the observed deletion in the mutant (Figure 3). However, this deletion did not affect the transcription level of *PaCdk5*, which was similar to the one of *PaCdk5* in the wild type (Figure 4). This result, together with the absence of mutations in the *PaCdk5* predicted CDS in the *PaTim54*^{2218} mutant pointed to a role of *PaTim54* in the specific phenotype of the *PaTim54*^{2218} mutant.

3.4. *PaCdk5* and *PaNip30* loss-of-functions are not responsible for the *PaTim54*^{2218} phenotypes

With the aim to test the role of *PaCdk5* and *PaNip30* in *P. anserina*, we Knocked Out (K.O) *PaCdk5* and *PaNip30* separately and we also generated the double *ΔPaCdk5 ΔPaNip30* K-O strain (see materials and methods). *PaCdk5* CDS was replaced by a hygromycin B resistance cassette while *PaNip30* CDS was replaced by a nourseothricin resistance (nouR) cassette (Figure S1). While the *ΔPaNip30* strain was strictly identical to the wild type, mycelium in the *ΔPaCdk5* as well as in the

double *ΔPaCdk5 ΔPaNip30* mutant strains was slightly more pigmented and with less aerial hyphae (Figure 1). Importantly, the vegetative mutant phenotype of *ΔPaCdk5* and of *ΔPaCdk5 ΔPaNip30* was clearly distinguishable from the one of *PaTim54*^{2218}. Wild-type vegetative phenotype was restored (3 [WT] out of 12 [phleoR]) when *ΔPaCdk5 was* co-transformed with pPaCdk5 and pBC-phleo (conferring resistance to phleomycin) together but not when transforming pBC-phleo alone (0 [WT] out of 15 [phleoR]). Complementation of *ΔPaCdk5* in the *ΔPaCdk5 ΔPaNip30* double mutant was achieved by crossing the *ΔPaCdk5 ΔPaNip30* double mutant with a [WT] *PaTim54*^{2218} *pPaCdk5 pBC-phleo* transformant. Phenotypic analyses of the progeny showed that the *pPaCdk5* and the *pBC-phleo* transgenes were co-integrated in the genome as often observed in *P. anserina* (Razanamparany and Bégueret, 1988) and that the *ΔPaCdk5 ΔPaNip30 pPaCdk5 pBC-phleo* progeny presented wild-type phenotype. These data argued that only deletion of *PaCdk5* accounted for the mutant vegetative phenotype in *ΔPaCdk5* as well as in *ΔPaCdk5 ΔPaNip30.* HI was as in the wild type for the three K.O strains tested: *ΔPaCdk5, ΔPaNip30* and *ΔPaCdk5 ΔPaNip30* (Figure 1). In conclusion, *PaNip30* has no role in the processes studied here and *PaCdk5* loss-of-function did not account for the *PaTim54*^{2218} phenotypes.

3.5. *PaCdk5* does not *trans*-complement *PaTim54*^{2218}

The absence of mutation in *PaCdk5* CDS, its unaffected expression in *PaTim54*^{2218} as well as the phenotype of *ΔPaCdk5* were in sharp contrast to the observed complementation of *PaTim54*^{2218} when this latter was transformed with *PaCdk5* wild-type copy bearing transgenes. This led us to hypothesize that the integration sites of the transgenes might account for this discrepancy. We thus investigated genetic linkage between the *pBC-hyg-PaCdk5* transgenes and the *PaTim54*^{2218} mutation in three of the "complemented" [WT] *PaTim54*^{2218} *pBC-hyg-PaCdk5* mentioned before by crossing them with the wild type (Table 2). Strikingly, no meiotic recombination was observed between the *pBC-hyg-PaCdk5* integrated transgenes and the *PaTim54*^{2218} mutation in the three crossings. The χ^2 statistical analysis of the F1 progeny phenotypes distribution argued that for the three parental transformants analyzed, the *pBC-hyg-PaCdk5* transgenes were genetically linked to the *PaTim54*^{2218}

mutation ($P<10^{-2}$). Similar genetical analyses revealed that in the [WT, hygR] transformants co-transformed with *PaCdk5*^{PCR} and pBC-hyg, both elements co-integrated and were genetically linked to *PaTim54*^{2218} mutation (data not shown). Altogether, this indicated that the *PaCdk5* bearing transgenes could "complement" *PaTim54*^{2218} only when inserted in *cis* close to the *PaTim54*^{2218} locus (Figure 1). This result was intriguing for *bona fide* functional complementation relies on "*in trans*" rescue of the loss-of-function of a gene by its wild-type copy. We hence addressed the question whether pPaCdk5 could *trans*-complement *PaTim54*^{2218}. In a first step, three independent [WT] complemented *ΔPaCdk5 pPaCdk5 pBC-phleo* strains were crossed with the wild type (Table 3). In the progeny of the three crossings, [hygR phleoR] spores presented a [WT] phenotype while the [hygR phleoS] progeny conserved a mutant [ΔPaCdk5] phenotype. In addition, equal distribution of the four different phenotypic categories showed genetic independence between both *loci*, leading us to conclude to ectopic chromosomal co-integration of both *pPaCdk5* and *pBC-phleo* (χ^2analysis: P>0.05). We then tested if these transgenes could *trans*-complement *PaTim54*^{2218} by crossing one *ΔPaCdk5 pPaCdk5 pBC-phleo* F1 progeny from each parent transgenic line with *PaTim54*^{2218} (Table 4). Strikingly, none of the *PaTim54*^{2218} *pPaCdk5 pBC-phleo* progeny genotype presented a wild-type phenotype (annotated *PaTim54*^{2218} *pPaCdk5 pBC-phleo-trans* in Figure 1). This demonstrated that wild-type copy of *PaCdk5* did not *trans*-complement *PaTim54*^{2218} although the *pPaCdk5* transgenes were functional.

Inversely, we wondered whether some *pPaCdk5* transgenes in "non-complemented" [PaTim54^{2218}] *PaTim54*^{2218} *pPaCdk5 pBC-phleo* transformants were actually functional but that they did not complement *PaTim54*^{2218} because they were ectopically integrated. To this aim, we crossed two independent non complemented [PaTim54^{2218}] *PaTim54*^{2218} *pPaCdk5 pBC-phleo* transformants to *ΔPaCdk5* (Table S3). Progeny analysis for both transformants showed that, first, *pPaCdk5 and pBC-phleo* were ectopically co-integrated (no genetic linkage between the *PaCdk5/PaTim54*^{2218} locus and the transgenes integration sites; χ^2analysis: P>0.05) and second that the *pPaCdk5* transgenes previously shown as unable to complement *PaTim54*^{2218} did complement *ΔPaCdk5*. Indeed, in both

crossings, the *ΔPaCdk5 pPaCdk5 pBC-phleo* progeny presented wild-type phenotype. In addition, one [PaTim54^{2218}] *PaTim54^{2218} pPaCdk5 pBC-phleo* transformant was crossed to the double *ΔPaCdk5 ΔPaNip30* mutant (Table S4). In the progeny, the *ΔPaCdk5 ΔPaNip30 pPaCdk5 pBC-phleo* descendants showed wild-type phenotype, demonstrating as mentioned before that only *PaCdk5* loss-of-function was responsible for the [pPaCdk5] mutant phenotype in *ΔPaCdk5 ΔPaNip30.*

Altogether, these data argued that the *PaTim54^{2218}* mutation was not functionally *trans*-complemented by wild-type *pPaCdk5* but rather genetically *cis*-suppressed by genetically linked *pPaCdk5*-bearing transgenes (Figure 1). Importantly, the *PaCdk5^{PCR}* fragment allowing *cis*-suppression of *PaTim54^{2218}* mutation in the co-transformation experiments mentioned above does not span the *PaTim54^{2218}* deletion (Figure 3).

3.6. *PaTim54* is the gene affected in *PaTim54^{2218}*

Hence, the most likely candidate gene for being altered in *PaTim54^{2218}* remained *PaTim54*. Similarly as what we did for the pBC-hyg-PaCdk5 transgenes, we first tested the genetic linkage between the *pBC-hyg-PaTim54* integrated transgenes and the *PaTim54^{2218}* locus in three independent [WT] *PaTim54^{2218} pBC-hyg-PaTim54* complemented transformants by crossing them with the wild type. As reported in Table 5, [hygS] progeny showed [*PaTim54^{2218}*] mutant phenotype while all the [hygR] descendants showed wild-type phenotype. First, this confirmed the capacity of the *pBC-hyg-PaTim54* transgenes analyzed to complement *PaTim54^{2218}*. Second, χ^2 statistical analysis of the F1 progeny phenotypes distribution determined that in every transformants, the *pBC-hyg-PaTim54* inserted transgene and the *PaTim54^{2218}* mutation were genetically independent (P>0.05). This led us to conclude that *PaTim54* wild-type copy did functionally *trans*-complement *PaTim54^{2218}*. Altogether, these data showed that *PaTim54* was the gene affected in *PaTim54^{2218}*.

3.7. *PaTim54* is essential in *P. anserina*

First identified in *S. cerevisiae* as an essential gene by Kerscher *et al*. (Kerscher et al., 1997), other groups eventually obtained viable *tim54* deleted strains (Hwang et al., 2007; Kovermann et al., 2002). We attempted to delete *PaTim54* to functionally assess *PaTim54* loss-of-function. A *Δmus51* strain (inactivated for the NHEJ repair system; see materials and methods), was transformed with a hygromycin B-resistance cassette designed to delete *PaTim54* and we obtained 40 [hygR] transformants with no mutant vegetative phenotype. For twelve of these [hygR] transformants, integration of the deletion cassette was tested and validated by PCR (see materials and methods). Four of these validated transformants were crossed with the wild type to obtain pure homokaryotic *ΔPaTim54* (devoid of *Δmus51*) in the F1 progeny. In *P. anserina*, two kinds of ascospores can be found in *asci*. In a minority of *asci*, small homokaryotic ascospores can be recovered (along with large self-fertile dikaryotic ascospores), while the vast majority of *asci* only present four large *mat+/mat-* self-fertile dikaryotic ascospores. None of the four crossings yielded homokaryotic [hygR] *ΔPaTim54* progeny. However, second division segregation (SDS) asci containing 4 [hygR] dikaryotic ascospores could be recovered. These asci contained self-fertile dikaryotic ascospores of the *mat+/mat- ΔPaTim54*/+ genotype that gave rise to wild-type growing mycelium. We then harvested homokaryotic progeny from two different self-fertile dikaryotic *mat+/mat- ΔPaTim54*/+ strains. For the first strain, only 18 [hygS] out of 36 ascospores germinated and for the second strain, 14 [hygS]/ 36 harvested ascospores germinated. All together, these data suggested that *ΔPaTim54* deletion was lethal and/or impaired for ascospore germination, and both phenotypes being recessive.

Since homokaryotic *ΔPaTim54* could not be obtained, we could not verify the strain by Southern blotting but we validated *PaTim54* loss-of-function by complementation. To this purpose, we generated a pBC-phleo-PaTim54 plasmid by subcloning wild-type *PaTim54* from pPaTim54 into pBC-phleo. In a first step, this pBC-phleo-PaTim54 plasmid was transformed into $PaTim54^{2218}$ and we obtained 46 [WT] complemented out of 54 [phleoR] transformants. We assumed that in these complemented transformants, the *pBC-phleo-PaTim54* transgenes were functional. We then transferred the *pBC-phleo-PaTim54* transgenes in a *ΔPaTim54* strain in two steps. First, we used the

[hygR] *mat+/mat- ΔPaTim54*/+ self-fertile dikaryotic ascospores, (see above) to determine the mating type of the nucleus carrying the *ΔPaTim54* deletion. To this purpose, we crossed one *mat+/mat- ΔPaTim54*/+ with both the *mat+* and the *mat-* wild-type strains. As shown in Table 6, only crossing with the *mat-* wild type partner yielded SDS asci with four *ΔPaTim54*/+ spores, arguing that in the analyzed *mat+/mat- ΔPaTim54*/+ strains, the *ΔPaTim54* deletion was carried by the *mat+* nucleus (Table 6). Then, we crossed the [hygR] mat+/mat- *ΔPaTim54*/+ strain carrying the *ΔPaTim54* deletion in the *mat+* nucleus with a [WT phleoR] *mat- PaTim54^{2218} pBC-phleo-PaTim54* strain (Table 7). In the progeny, we harvested [WT hygR phleoR] viable homokaryotic *ΔPaTim54 pBC-phleo-PaTim54* as well as viable dikaryotic *ΔPaTim54/ΔPaTim54 pBC-phleo-PaTim54/+* descendants. Notably, the χ^2 statistical analysis did not indicate genetic linkage between *PaTim54* and the different *pBC-phleo-PaTim54* transgenes studied (P>0.05). When tested for HI, the *ΔPaTim54 pBC-phleo-PaTim54* progeny was comparable to the wild type (Figure 1). These data confirmed that wild-type *PaTim54* fully *trans*-complemented *ΔPaTim54*. Finally, to test whether *PaTim54* was essential in *P. anserina*, we proceeded to mycelium fragmentation of one *ΔPaTim54/ΔPaTim54 pBC-phleo-PaTim54/+* dikaryotic strain (see materials and methods). After mycelium regeneration, we recovered sixty [HygR phleoR] *ΔPaTim54/ΔPaTim54 pBC-phleo-PaTim54/+* dikaryotic thalli, fourteen homokaryotic [hygR phleoR] *ΔPaTim54 pBC-phleo-PaTim54* thalli but no homokaryotic [hygR phleoS] *ΔPaTim54*. This latter result strongly argued that deletion of *PaTim54* was lethal and more specifically that *PaTim54* was essential for mycelial growth in *P. anserina*.

3.8. *PaTim54* gene expression is affected in *PaTim54^{2218}*

Because the sequence of the *PaTim54* CDS was not altered in *PaTim54^{2218}*, we hypothesized that its expression may be affected in the mutant. To address this question, we tested *PaTim54* gene expression by RT-qPCR. Strikingly, *PaTim54* mRNA level was less than 10% of the wild-type level in *PaTim54^{2218}* as well as in *PaTim54^{2218} pPaCDk5 pBC-phleo-trans*, two strains harboring [PaTim54^{2218}] mutant phenotype (Figure 4). On the contrary, *PaTim54* gene expression was like the wild type in the other strains tested except in the complemented *PaTim54^{2218} pBC-phleo-PaTim54* strain, where

PaTim54 expression fold-change was 1.9 compared to wild type, suggesting that overexpression of *PaTim54* in this strain restored wild-type phenotype. Interestingly, *PaTim54* expression was reduced to 23 % of the wild-type level in the *PaTim54^{2218} pBC-hyg-PaCdk5-cis* transformant although this strain exhibited a wild-type phenotype. In contrast, *PaTim54* expression in *ΔPaCdk5*, in *ΔPaNip30* and in the double *ΔPaCdk5 ΔPaNip30* K-O strains was not statistically different from the wild type suggesting that the gene replacements operated in these strains did not disturb *PaTim54* expression. It is worthy to note that *PaCdk5* gene expression was not down-regulated either in *PaTim54^{2218} pBC-phleo-PaTim54,* in *PaTim54^{2218} pPaCdk5 pBC-phleo-trans* or in *PaTim54^{2218} pBC-hyg-PaCdk5-cis.* Altogether, these data strongly argued that only very low *PaTim54* gene expression level was responsible for the pleiotropic [PaTim54^{2218}] mutant phenotypes.

3.9. *PaMpk1* regulates *PaTim54^{2218}*-triggered oxidative burst

As shown in Figure 1, we could detect a massive oxidative burst at the confrontation between *PaTim54^{2218}* and *P. chrysogenum* during HI. However, cell death at the confrontation in *P. chrysogenum* revealed by Evans blue staining was abolished compared to that when the wild type was challenged with *P. chrysogenum*. The PaMpk1 MAP Kinase pathway as well as the PaNox1 complex are important regulators of HI in *P. anserina*. Indeed, the oxidative burst along with cell death in *P. chrysogenum* at the confrontation are both abolished when *ΔPaMpk1* and *PaNox1^{-}* mutants are challenged (Figure 1) (Silar, 2005). In order to determine whether *PaMpk1* and *PaNox1* could play a role in *PaTim54^{2218}*-triggered HI, we constructed the *PaTim54^{2218} ΔPaMpk1* as well as the *PaTim54^{2218} PaNox1^{-}* double mutants. Interestingly, mycelium in both double mutant strains neither looked alike *PaTim54^{2218}*, nor *ΔPaMpk1* or *PaNox1* parental strains. On the contrary, mycelium in both double mutant strains was scarce (Figure 1). This observation that mycelium in both double mutant strains was more severely affected than in the single suggested a synergistic interaction between *PaTim54^{2218}* and *ΔPaMpk1* as well as between *PaTim54^{2218}* and *PaNox1^{-}* regarding vegetative growth. With the aim to assay HI in *PaTim54^{2218} ΔPaMpk1* and *PaTim54^{2218} PaNox1^{-}* double mutants, we challenged both strains with *P. chrysogenum*. We observed that cell death in *P.*

chrysogenum at the confrontation with *PaTim54^{2218}, PaNox1^{-},* and *ΔPaMpk1* single mutants was abolished as previously shown (Figure 1). The result was similar for *PaTim54^{2218} ΔPaMpk1* and *PaTim54^{2218} PaNox1^{-}* double mutants. DAB staining was slightly decreased in *PaTim54^{2218} PaNox1^{-}* double mutant while it was strongly reduced in *PaTim54^{2218} ΔMpk1* double mutant compared to in the wild type. Hence, *ΔPaMpk1* mutation was clearly epistatic over *PaTim54^{2218}* mutation, while *PaNox1^{-}* mutation was only partially epistatic over the *PaTim54^{2218}* mutation. Since vegetative growth in both double mutants was similarly affected, both showing scarce and flat mycelium (Figure 1), the fact that DAB staining in *PaTim54^{2218} PaNox1^{-}* when challenged with *P. chrysogenum* was just slightly decreased argued that drastic DAB staining loss observed in *PaTim54^{2218} ΔMpk1* when challenged with *P. chrysogenum* was unlikely due to reduced mycelium density or growth defects. This led us to conclude to a major role of the PaMpk1 MAPK, in contrast to the PaNox1 NADPH oxidase that may have a limited role, in regulating the massive oxidative burst triggered in *PaTim54^{2218}*.

3.10. *PaTim54^{2218}* mutation affects the mitochondrial network

With the aim to investigate the mitochondrial network in *PaTim54^{2218}* when grown on standard medium but also when challenged with *P. chrysogenum*, we constructed a *PaTim54^{2218} mito-GFP* (Sellem et al., 2007). In yeast, Tim54p is involved in the import of proteins of the inner membrane and it has been shown that null mutation of *tim54* does not affect import of soluble matrix proteins (Kerscher et al., 1997). Accordingly, GFP fluorescence intensities measured in the *PaTim54^{2218} mito-GFP* strain were not statistically different than in the *mito-GFP* control strain arguing for a normal import of the soluble matrix mito-GFP reporter protein in *PaTim54^{2218}* mutant background (Figure S3). To standardize our cytological analyses, we focused on hyphae of the growing edge of the thallus. Indeed, mitochondrial morphology is highly dynamic, with mitochondria forming long longitudinal tubes in the apical hyphae (thread-like network) to shorter tubes and finally rounded mitochondria in the central part of the thallus (data not shown). We thus analyzed GFP tagging pattern at the edge of the thallus in the *PaTim54^{2218} mito-GFP* tagged strain and we compared it to the control strain bearing only the *mito-GFP* transgene as well as to the complemented *PaTim54^{2218}*

593 *pBC-phleo-PaTim54 mito-GFP* strain. Green fluorescence pattern in the control strain as well as in the
594 complemented *PaTim54^{2218} pBC-phleo-PaTim54 mito-GFP* strain exhibited a thread-like
595 mitochondrial network formed of highly tubular and easily trackable mitochondria (Figure 5A). On
596 the contrary, GFP tagging pattern in *PaTim54^{2218} mito-GFP* was much more intricate. Mitochondria in
597 the mutant looked shorter, thinner, and somehow packed, as if filling the cytoplasm. They did not
598 form long tubular structures as in the control and in the complemented strain. In addition to the size
599 difference, we also determined that their diameter was significantly smaller (334 ± 37 nm; t-test:
600 $P<10^{-9}$) in *PaTim54^{2218}* compared to the control (456 ± 52 nm) and the complemented strain (418 ± 60
601 nm; t-test: $P<10^{-5}$).

602 We also analyzed the mitochondrial network at the edge of the thallus when *P. anserina* was
603 challenged with *P. chrysogenum*. For both the *mito-GFP* control strain as well as for *PaTim54^{2218}*
604 *mito-GFP*, tagging pattern in hyphae in close contact to *P. chrysogenum* was not different from the
605 tagging pattern in hyphae of the growing edge without challenge (Figure 6). This indicated that
606 challenging with *P. chrysogenum* did not significantly affect *P. anserina* mitochondrial network at the
607 confrontation. However, we often observed small lateral branching hyphae that swelled in
608 *PaTim54^{2218}* (Figure 6). When laterally branching hyphae were observed in the control, they exhibited
609 standard morphology but no swelling. This latter observation indicated that the challenge with *P.*
610 *chrysogenum* did induce swelling of small growing hyphae specifically in *PaTim54^{2218}*.

611 **3.11. *PaTim54^{2218}* mutation affects nucleoids**

612 In *S. cerevisiae*, it has been shown that the number of nucleoids, the structure where the
613 mitochondrial DNA (mtDNA) is found, was decreased in the *tim54* mutant strains (Hwang et al.,
614 2007). In order to assay mtDNA stability in *P. anserina*, we quantified mtDNA by qPCR and we
615 cytologically analyzed the distribution of nucleoids on young mycelium. Samples were stained with
616 DAPI and the number of nucleoids in 10 µm length hyphal segments was quantified (Figure 5A).
617 Surprisingly, the number of nucleoids in *PaTim54^{2218} mito-GFP* was dramatically increased compared

to the *mito-GFP* control (32 ± 9 in *PaTim54^{2218} vs.* 9 ±3 in the control; t-test: P<10^{-9}) and to the *PaTim54^{2218} pBC-phleo-PaTim54 mito-GFP* complemented strain (12 ± 4; t-test<10^{-8}) (Figure 5B). Interestingly, these nucleoids were significantly smaller in *PaTim54^{2218} mito-GFP* than in the control (313 ± 72 nm in *PaTim54^{2218} vs.* 429 ± 75 nm in the control; t-test: P<10^{-4}) and in the complemented strain (416 ± 53 nm; t-test<10^{-4}) (Figure 5C). These observations suggested that the nucleoids in *PaTim54^{2218} mito-GFP* were somehow disorganized and likely fragmented. However, these data did not allow us to conclude on the stability of the mtDNA in *PaTim54^{2218}*. To this aim, the ratio of mtDNA versus nuclear DNA in young mycelium was measured by qPCR in *PaTim54^{2218}*, *PaTim54^{2218} pBC-phleo-PaTim54* and the wild type (Figure 7A). The level of mtDNA was similar in the three tested strains, leading us to conclude that the important accumulation of nucleoids of small size in *PaTim54^{2218}* was indicative of disorganization and/or fragmentation of nucleoids but not of increased mtDNA level. Importantly, we determined that senescent DNA (senDNA) was absent in the DNA samples used for the mtDNA level quantification (Figure 7B), which is in agreement with the paradigm that senDNA is absent in young mycelium (Osiewacz et al., 2010). This suggested that senDNA did not account for disorganized and/or fragmented nucleoids observed in *PaTim54^{2218}* young mycelium and this indicated that senDNA did not alter mtDNA level quantifications. Finally, the fact that the number of nucleoids, their size as well as the quantity of mtDNA in the *PaTim54^{2218} pBC-phleo-PaTim54* complemented strain were similar to the wild type, emphasized that all the defects evidenced above in *PaTim54^{2218}* are due to the *PaTim54^{2218}* hypomorphic allele.

3.12. *PaTim54^{2218}* mutation affects the *PaAOX* gene expression level and longevity in *P. anserina*

P. anserina is a potent model system to study aging (Marcou, 1961; Osiewacz et al., 2010). Indeed, contrary to many filamentous fungi, *P. anserina* vegetative growth is limited to about 10 cm (about 15 to 20 days of growth) on standard M2 medium and at standard temperature (27°C). This phenomenon is known as senescence (Rizet, 1953b). To study senescence in the wild type, in *PaTim54^{2218}* as well as in the *PaTim54^{2218} pBC-phleo-PaTim54* complemented strain, we analyzed the growth distance of mycelium cultures from freshly germinated spores (Figure 8). In these longevity

644 assays, all the cultures of the wild type as well as of the *PaTim54*^{2218} *pBC-phleo-PaTim54*
645 complemented strains died after an average of 10 cm of growth, corresponding to about 15-20 days
646 of longevity. On the contrary, 12/18 cultures of the *PaTim54*^{2218} genotype and corresponding to three
647 replicates from three single *mat+* ascospores and one single *mat*- ascospore were still growing after
648 191 days of incubation for a total growth distance of approximately 1 m, a longevity never observed
649 in *WT*. Statistical analysis supported the difference observed between the *PaTim54*^{2218} strain and the
650 *WT* or the *PaTim54*^{2218} *pBC-phleo-PaTim54* complemented strains (Figure 8; $P<4.10^{-8}$). Worth is to
651 note that these cultures were still growing when measurements were stopped. Remarkably, the
652 three replicates from two individual *mat + PaTim54*^{2218} spores underwent senescence after an
653 average of 22 and 25 cm growth distance respectively. This indicated that senescence was not
654 completely abolished in *PaTim54*^{2218}. Nevertheless, these longevity assays demonstrated that
655 *PaTim54*^{2218} behaved as a long-lived mutant and that *PaTim54*^{2218} hypomorphic allele was
656 responsible for increased longevity.

657 *P. anserina* is an obligate aerobe fungus in which respiratory mutants lacking Cytochrome c oxidase
658 activity (*E.g PaCOX1* and *PaCOX5* mutants) are nonetheless viable but they astonishingly show
659 strikingly increased lifespan. In such mutants, overexpression of the alternative oxidase encoding
660 gene *PaAOX* has been shown to compensate for the lack of Cytochrome c oxidase activity and the
661 exclusive use of the alternative respiration pathway that produces less reactive oxygen species leads
662 to increased lifespan (Dufour et al., 2000; Lorin et al., 2001; Sellem et al., 2007). In order to test
663 whether the Cytochrome c respiratory pathway was disturbed in *PaTim54*^{2218}, we quantified the
664 expression of the *PaAOX* gene by RT-qPCR. Strikingly, strains harboring [PaTim54^{2218}] phenotypes,
665 namely *PaTim54*^{2218} and *PaTim54*^{2218} *pPaCdk5 pBc-phleo-trans*, exhibited potent overexpression of
666 the *PaAOX* gene, the hallmark of Cytochrome c respiratory pathway mutants (Figure 4). In particular,
667 the *PaTim54*^{2218} mutant showed a *PaAOX* gene expression fold-change of ten compared to wild type.
668 In the other strains tested and especially in the [WT] *PaTim54*^{2218} *pBC-phleo-PaTim54* complemented

669 strain, *PaAOX* gene expression was like in the wild type. This last result strongly suggested that the
670 *PaTim54*^{2218} mutation impaired the respiratory chain.

671 **4. Discussion**

672 **4.1. *The PDC*^{2218} mutant and Hyphal Interference**

673 Microbial communities are complex ecosystems where interplay between fungi, bacteria and
674 invertebrates such as nematodes are of major importance (Crowther et al., 2012; De Boer et al.,
675 2005). Interactions can be of different kinds and in this paper we focused on Hyphal Interference
676 (HI), a defense response shown by filamentous fungi when their hyphae directly contact a competitor
677 fungus. This implies that fungi capable of HI i) can sense the competitor's hyphae, ii) recognize them
678 as non-self and iii) are endowed with an appropriate downstream signaling pathway and effectors
679 required to trigger the HI response. The ascomycete fungus *P. anserina* is able to display a HI
680 response when challenged with various fungal competitors; however the basidiomycete *Coprinopsis*
681 *cinera* is able to kill *P. anserina* hyphae, while *P. anserina* is able to kill *P. chrysogenum* (Silar, 2005).
682 Non-self-recognition not only in *P. anserina* but more generally in the fungal kingdom is largely
683 unknown. First involved in cell death during Vegetative Incompatibility in *P. anserina* and in *N.*
684 *crassa*, Nucleotide Oligomerization Domain (NOD)-like Receptors (NLRs) could play the role of
685 Pattern Recognition Receptors (PRRs) in fungi (Bidard et al., 2013; Lamacchia et al., 2016; Paoletti,
686 2016; Uehling et al., 2017). Nowadays, only Het-C in *N. crassa, "*the host"*,* has been shown as a true
687 PRR able to bind the PhcA protein from *Pseudomonas syringae,* the "pathogen", and to trigger cell
688 death in the host (Wichmann et al., 2008). How *P.anserina* recognizes non-self-hyphae is an open
689 question. Similarly, it is not clear how cell death in the challenger, here *P. chrysogenum*, is triggered.
690 Fungi are able to produce many kinds of toxic compounds in order to kill their competitors. Among
691 the list of active antifungal compounds able to trigger hyphal death are secondary metabolites,
692 volatile organic compounds, small secreted polypeptides and secreted lytic enzymes (Silar, 2012). A
693 burst of Reactive Oxygen Species (ROS) is generated on the thallus of *P. anserina* when challenged by

694 different fungal species. However, these ROS are unlikely directly responsible for *P. chrysogenum* cell
695 death. Indeed, the *PDC*^{2218} mutant analyzed here shows an increased oxidative burst and triggers less
696 death in the competitor. On the same line, we have previously shown that the ROS produced by the
697 PaNox1 NADPH oxidase are involved in signaling rather than in killing during HI (Brun et al., 2009).
698 Interestingly, epistasis analysis shows that PaNox1 only plays a minor role in the oxidative burst
699 displayed by *PDC*^{2218}*.* The additional sources of these ROS remain to be identified. Epistasis data
700 indicate that their production in *PDC*^{2218} is under the control of the CWI PaMpk1 MAP kinase
701 pathway.

702 We want to stress the point that Nox1 and the Mpk1 MAP Kinase pathway control virulence in
703 mycoparasitic *Trichoderma sp.* developed for biocontrol of fungal plant pathogens as well
704 (Druzhinina et al., 2011; Karlsson et al., 2017). For instance, the Nox1 NADPH oxidase of *Trichoderma*
705 *harzanium* and the ROS it produces are important in the biocontrol of the phytopathogen *Phytium*
706 *ultimum* (Montero-Barrientos et al., 2011). In the closely related species *Trichoderma virens*, the
707 TmkA (=Tvk1) and TmkB MAP kinases, homologous to PaMpk2 and PaMpk1 respectively, play key
708 roles in the mycoparasitic activity against *Sclerotium rolfsii*, *Rhizoctonia solani* and *Phytium spp.*
709 (Kumar et al., 2010; Mukherjee et al., 2003). HI and mycoparasitism may be closely related processes
710 relying on a common set of regulatory pathways.

711 **4.2. The *PDC*^{2218} phenotypes result from transcriptional down-regulation of *PaTim54***

712 Following classical genetic cartography and positional cloning procedures, we characterized a 1560
713 bp deletion as responsible for the pleiotropic phenotypes in the *PDC*^{2218} mutant. This deletion
714 identified in *PDC*^{2218} genome removes the 5' end of *PaNip30*, a putative gene with unknown function,
715 together with most of the putative 3'UTR of *PaCdk5*, the homologue of the yeast cyclin-dependent-
716 kinase *Cdk5*. Several arguments immediately ruled out the possibility that *PaNip30* was the gene
717 affected in *PDC*^{2218}. Additionally, several strong arguments, especially complementation of *PDC*^{2218}
718 with a wild-type copy of *PaCdk5*, suggested that *PaCdk5* might be the gene affected in *PDC*^{2218}.

However, targeted gene deletion and *cis*- versus *trans*-complementation and functional complementation experiments supported by Mendelian genetic analyses pointed to *PaTim54* as the only gene affected in *PDC*^{2218}. Although *PaCdk5* deletion points to a role of this putative cyclin in aerial hyphae production as well as mycelial pigmentation in *P. anserina* as well, we want to emphasize that *PaTim54* fully restores wild-type phenotypes in *PaTim54*^{2218} mutants (*i.e*, aerial hyphae, pigmentation, growth rate, thermosensitivity, longevity, mitochondrial defects and hyphal Interference) arguing that only *PaTim54* function is altered in *PaTim54*^{2218} mutants. We eventually show that *PaTim54* is essential in *P. anserina* and that *PaTim54*^{2218}, the allele present in *PDC*^{2218}, is hypomorphic and triggers low level of expression of *PaTim54*. There is no evidence to explain the down-regulation in *PaTim54* gene expression or the cis-suppressing effect of *PaCdk5* bearing transgenes. Further investigations including genome sequencing of several *cis*-suppressed [WT] *PaTim54*^{2218} *pBC-hyg-Cdk5* transformants will be required to understand this *cis*-suppression effect of *PaCdk5* bearing transgenes. However; since transformation of *PaTim54*^{2218} with *PaCdk5*^{PCR}, a PCR fragment not overlapping the *PaTim54*^{2218} deletion, leads to *cis*-suppression as well, we assume that *cis*-suppression by *PaCdk5* bearing transgenes does not rely on the comeback of missing regulatory sequences controlling *PaTim54* expression and deleted in *PaTim54*^{2218}.

4.3. *PaTim54*, mitochondria and defense response

The *PaTim54* gene encodes the orthologue of the yeast mitochondrial Translocase of the inner Membrane Tim54p (Kerscher et al., 1997). PaTim54 protein shares 60% and 40% identity with *N. crassa* and *S. cerevisiae* Tim54p proteins, respectively. Noteworthy, no other homologue has been found in the *P. anserina* genome. Similarly to the yeast *tim54* mutants, *PaTim54*^{2218} shows slow growth at cold temperature (18°C) and thermal sensitivity at 37°C. However, while the yeast Tim54p has no major role in mitochondrial morphology, *PaTim54*^{2218} mutation promotes significant mitochondrial fission. Indeed, cytological analysis of mitochondria in living cells shows that the

744 thread-like mitochondrial network is altered in *PaTim54*^{2218}. This mitochondrial morphology change
745 in *PaTim54*^{2218} is reminiscent of increased mitochondrial fission and/or decreased mitochondrial
746 fusion. In addition in the *tim54* yeast mutants, the number of nucleoids is decreased (Hwang et al.,
747 2007). Although we have observed that the number of nucleoids is dramatically increased in
748 *PaTim54*^{2218}, mtDNA level remains unchanged. Hence, the *PaTim54*^{2218} allele seems to promote the
749 disorganization and fragmentation of nucleoids but not mtDNA degradation in *P. anserina*.

750 A growing body of evidence links mitochondria to immunity. In humans, several immune syndromes
751 are now considered as "likely" due to primary mitochondrial disorders like the Barth Syndrome or the
752 Cartilage Hair Hypoplasia. It becomes clear that mitochondria participate in RLR signaling (an antiviral
753 response based on RLR-Retinoic acid Like Receptor), antibacterial immunity and inflammation
754 (Walker et al., 2014; West et al., 2011). Noteworthy, both the mitochondrial ROS production as well
755 as the capacity of mitochondria to fuse are two important phenomena involved in RLR signaling and
756 inflammation, respectively. Signaling responses to non-self through mitochondria appears thus
757 conserved during evolution. We show here that the *P. anserina* mitochondrial network is not
758 modified in hyphae in close contact with hyphae of competing fungus during HI. However, we show
759 that *PaTim54* function is required for the down-regulation of the oxidative burst during HI and to
760 trigger hyphal cell death in the challenging fungus. Hence, like the PaMpk1 and the PaNox1 signaling
761 pathways, mitochondria appear as important actors of HI. Further studies will be required to
762 understand how mitochondria and the PaMpk1 pathway interact in the regulation of the HI response
763 in *P. anserina*.

764 **4.4. *PaTim54*, mitochondria and aging**

765 Mitochondria play a major role in aging in a wide range of eukaryotes as well. This organelle is known
766 to provide the cell with ATP through the respiratory chain. However, the byproducts of this process,
767 namely the ROS, are able to damage cellular components such as proteins, nucleic acids and lipids.
768 This damaging capacity of mitochondria-produced ROS is well known as the "Mitochondrial Free

769 Radical Theory of Aging" (Harman, 1972). However, ROS production is not anymore considered as
770 the only way mitochondria impact cell longevity. Evidences show that several regulatory pathways
771 merging in a quality control system in mitochondria influence lifespan as well (Osiewacz, 2011;
772 Osiewacz et al., 2010; Osiewacz and Bernhardt, 2013). Briefly, this quality control includes ROS
773 scavenging, mtDNA maintenance, protein-repair, -refolding and -degradation, mitochondria shaping
774 (fusion vs. fission) and mitophagy (Fischer et al., 2012). In yeast, Tim54p is an integral protein of the
775 mitochondrial inner membrane with two predicted transmembrane domains. Tim54p participates in
776 at least two distinct complexes. On the one hand, it associates with the voltage dependent channel
777 protein Tim22p responsible for the import of integral membrane proteins. Although the role of
778 Tim54p in the complex remains unclear, Tim54p *per se* has been shown to be required for the
779 insertion/import of the Tim22p translocase, the ATP/ADP carrier Aac1p and the i-AAA protease
780 Yme1p, three intrinsic proteins of the mitochondrial inner membrane (Bolender et al., 2008; Kerscher
781 et al., 1997; Kovermann et al., 2002; Kurz et al., 1999). On the other hand, yeast Tim54p directly
782 interacts with the i-AAA-protease Yme1p (Hwang et al., 2007). Tim54p is absolutely required to
783 stabilize the 1M Da high molecular weight Yme1p complexes as well as for the protease activity of
784 the complex. Tim54p therefore plays a pivotal role in the import of proteins into mitochondria as
785 well as in their degradation (Hwang et al., 2007). Both roles may account for *PaTim54*^{2218} phenotypes.
786 We have shown that the *PaTim54*^{2218} mutation increases lifespan, a feature present in many
787 mitochondrial mutants. We have also demonstrated that mitochondrial morphology as well as
788 nucleoids organization are affected in the mutant. Noteworthy in *PaTim54*^{2218}, the increased lifespan
789 may not be correlated to a decrease in mitochondrial fission. Finally, as supported by *PaAOX* gene
790 overexpression in *PaTim54*^{2218} which is characteristic of lack of Cytochrome c oxidase function
791 (Dufour et al., 2000; Lorin et al., 2001; Sellem et al., 2007), insufficient *PaTim54* gene expression may
792 affect the respiratory chain function by disturbing import of its integral components (Kerscher et al.,
793 1997; Kovermann et al., 2002). It has been shown that Yme1p plays a major role in shaping
794 mitochondrial morphology and in mtDNA stability (Campbell et al., 1994). *N. crassa* IAP-1 and *P.*
795 *anserina* PaIAP, both orthologues of Yme1p, have previously been studied (Klanner et al., 2001; Weil

et al., 2011). As in yeast, IAP-1 and PaIAP are involved in proteolysis of misfolded proteins, participating in protein quality control (Osiewacz, 2011; Osiewacz et al., 2010). The *N. crassa iap-1* mutant strains show slow growth on non-fermentable carbon sources at high-temperature (40°C) and mutations in *PaIAP* leads to increased lifespan at normal temperature in *P. anserina*. Because of the similar lifespan increase in *PaTim54*^{2218} and in *PaIAP* mutants, it is tempting to speculate that both gene products may also work together in *P. anserina*. However, both mutant strains exhibit some differences in their phenotypes. For instance, *PaTim54* but not *PaIAP* is essential in *P. anserina.* Furthermore, the hypomorphic *PaTim54*^{2218} allele is thermosensitive in contrast to knocking-out *PaIAP* that slightly increases longevity at 37°C (Weil et al., 2011). This may be accounted for by a major role of Tim54p in protein import. Further studies of the role of *PaIAP* in Hyphal Interference as well as thorough studies of the double *PaTim54*^{2218} *ΔPaIAP* mutant in comparison with both single *PaTim54*^{2218} and *ΔPaIAP* mutants should give new insights into the role of both integral proteins of the mitochondrial inner membrane.

5. Conclusion

The characterization of the gene actually affected in the *PDC*^{2218} mutant has not been straightforward and *P. anserina* amenability for genetic analysis greatly helped us to differentiate “false positive” complementation (of *PaTim54*^{2218} by *PaCdk5*) from true trans-complementation of *PaTim54*^{2218} by *PaTim54,* thus evidencing that *PaTim54* was the actual gene whose decreased expression triggers the HI phenotypes. *In fine*, the study of the *PaTim54*^{2218} hypomorphic mutant gave us the opportunity to get insights into the functions of *PaTim54* in relation with defense and aging, although this gene is essential in *P. anserina*.

Funding

This work was funded by Université Paris-Diderot intramural funding.

Conflict of interest:

The authors declare that there are no conflicts of interest neither commercial affiliations.

Acknowledgments

We are greatly indebted to Pr. Annie Sainsard-Chanet and to Dr. Carole Sellem for their expertise in senescence in *Podsopora anserina*, to Sylvie Cangemi for technical help and to Charlène Girodet master student for her help. We want to thank the ImagoSeine facility, member of the France BioImaging infrastructure supported by the French National Research Agency (ANR-10-INSB-04, « Investmentsfit the future »).

References

Aguirre, J., Ríos-Momberg, M., Hewitt, D., Hansberg, W., 2005. Reactive oxygen species and development in microbial eukaryotes. Trends Microbiol. 13, 111–118. https://doi.org/10.1016/j.tim.2005.01.007

Bidard, F., Clavé, C., Saupe, S.J., 2013. The Transcriptional Response to Nonself in the Fungus *Podospora anserina*. G3amp58 GenesGenomesGenetics 3, 1015–1030. https://doi.org/10.1534/g3.113.006262

Boddy, L., 2000. Interspecific combative interactions between wood-decaying basidiomycetes. FEMS Microbiol. Ecol. 31, 185–194.

Boddy, L., Hiscox, J., 2016. Fungal Ecology: Principles and Mechanisms of Colonization and Competition by Saprotrophic Fungi. Microbiol. Spectr. 4. https://doi.org/10.1128/microbiolspec.FUNK-0019-2016

Bolender, N., Sickmann, A., Wagner, R., Meisinger, C., Pfanner, N., 2008. Multiple pathways for sorting mitochondrial precursor proteins. EMBO Rep. 9, 42–49. https://doi.org/10.1038/sj.embor.7401126

Boucher, C., Nguyen, T.-S., Silar, P., 2017. Species Delimitation in the Podospora anserina/ p. pauciseta/p. comata Species Complex (Sordariales). Cryptogam. Mycol. 38, 485–506. https://doi.org/10.7872/crym/v38.iss4.2017.485

Brun, S., Malagnac, F., Bidard, F., Lalucque, H., Silar, P., 2009. Functions and regulation of the Nox family in the filamentous fungus *Podospora anserina* : a new role in cellulose degradation. Mol. Microbiol. 74, 480–496. https://doi.org/10.1111/j.1365-2958.2009.06878.x

Campbell, C.L., Tanaka, N., White, K.H., Thorsness, P.E., 1994. Mitochondrial morphological and functional defects in yeast caused by yme1 are suppressed by mutation of a 26S protease subunit homologue. Mol. Biol. Cell 5, 899–905.

Crowther, T.W., Boddy, L., Jones, T.H., 2012. Functional and ecological consequences of saprotrophic fungus–grazer interactions. ISME J. 6, 1992–2001. https://doi.org/10.1038/ismej.2012.53

Cummings, D.J., McNally, K.L., Domenico, J.M., Matsuura, E.T., 1990. The complete DNA sequence of the mitochondrial genome of Podospora anserina. Curr. Genet. 17, 375–402. https://doi.org/10.1007/BF00334517

De Boer, W., B, F.L., C, S.R., Lynne, B., 2005. Living in a fungal world: impact of fungi on soil bacterial niche development⋆. FEMS Microbiol. Rev. 29, 795–811. https://doi.org/10.1016/j.femsre.2004.11.005

Debuchy, R., Brygoo, Y., 1985. Cloning of opal suppressor tRNA genes of a filamentous fungus reveals two tRNASerUGA genes with unexpected structural differences. EMBO J. 4, 3553–3556. https://doi.org/10.1002/j.1460-2075.1985.tb04116.x

DeVay, J.E., 1956. Mutual relationships in fungi. Annu. Rev. Microbiol. 10, 115–140.

Druzhinina, I.S., Seidl-Seiboth, V., Herrera-Estrella, A., Horwitz, B.A., Kenerley, C.M., Monte, E., Mukherjee, P.K., Zeilinger, S., Grigoriev, I.V., Kubicek, C.P., 2011. *Trichoderma*: the genomics of opportunistic success. Nat. Rev. Microbiol. 9, 749–759. https://doi.org/10.1038/nrmicro2637

du Prel, J.-B., Hommel, G., Röhrig, B., Blettner, M., 2009. Confidence Interval or P-Value? Dtsch. Ärztebl. Int. 106, 335–339. https://doi.org/10.3238/arztebl.2009.0335

Dufour, E., Boulay, J., Rincheval, V., Sainsard-Chanet, A., 2000. A causal link between respiration and senescence in Podospora anserina. Proc. Natl. Acad. Sci. 97, 4138–4143. https://doi.org/10.1073/pnas.070501997

El-Khoury, R., Sellem, C.H., Coppin, E., Boivin, A., Maas, M.F.P.M., Debuchy, R., Sainsard-Chanet, A., 2008. Gene deletion and allelic replacement in the filamentous fungus Podospora anserina. Curr. Genet. 53, 249–258. https://doi.org/10.1007/s00294-008-0180-3

Espagne, E., Lespinet, O., Malagnac, F., Da Silva, C., Jaillon, O., Porcel, B.M., Couloux, A., Aury, J.-M., Ségurens, B., Poulain, J., others, 2008. The genome sequence of the model ascomycete fungus Podospora anserina. Genome Biol. 9, R77.

Fischer, F., Hamann, A., Osiewacz, H.D., 2012. Mitochondrial quality control: an integrated network of pathways. Trends Biochem. Sci. 37, 284–292. https://doi.org/10.1016/j.tibs.2012.02.004

Glass, N.L., Jacobson, D.J., Shiu, P.K.T., 2000. The Genetics of Hyphal Fusion and Vegetative Incompatibility in Filamentous Ascomycete Fungi. Annu. Rev. Genet. 34, 165–186. https://doi.org/10.1146/annurev.genet.34.1.165

Haedens, V., Malagnac, F., Silar, P., 2005. Genetic control of an epigenetic cell degeneration syndrome in Podospora anserina. Fungal Genet. Biol. 42, 564–577. https://doi.org/10.1016/j.fgb.2005.03.011

Harman, D., 1972. The Biologic Clock: The Mitochondria? J. Am. Geriatr. Soc. 20, 145–147. https://doi.org/10.1111/j.1532-5415.1972.tb00787.x

Huang, D., Friesen, H., Andrews, B., 2007. Pho85, a multifunctional cyclin-dependent protein kinase in budding yeast. Mol. Microbiol. 66, 303–314. https://doi.org/10.1111/j.1365-2958.2007.05914.x

Hwang, D.K., Claypool, S.M., Leuenberger, D., Tienson, H.L., Koehler, C.M., 2007. Tim54p connects inner membrane assembly and proteolytic pathways in the mitochondrion. J. Cell Biol. 178, 1161–1175. https://doi.org/10.1083/jcb.200706195

Ikediugwu, F.E.O., 1976. Ultrastructure of hyphal interference between Coprinus heptemerus and Ascobolus crenulatus. Trans. Br. Mycol. Soc. 66, 281–290. https://doi.org/10.1016/S0007-1536(76)80054-X

Ikediugwu, F.E.O., Dennis, C., Webster, J., 1970. Hyphal interference by Peniophora gigantea against Heterobasidion annosum. Trans. Br. Mycol. Soc. 54, 307–309.

Ikediugwu, F.E.O., Webster, J., 1970. Hyphal interference in a range of coprophilous fungi. Trans. Br. Mycol. Soc. 54, 205-IN6. https://doi.org/10.1016/S0007-1536(70)80032-8

Iles, K.E., Forman, H.J., 2002. Macrophage signaling and respiratory burst. Immunol. Res. 26, 95–105. https://doi.org/10.1385/IR:26:1-3:095

Karlsson, M., Atanasova, L., Jensen, D.F., Zeilinger, S., 2017. Necrotrophic Mycoparasites and Their Genomes. Microbiol. Spectr. 5. https://doi.org/10.1128/microbiolspec.FUNK-0016-2016

Kerscher, O., Holder, J., Srinivasan, M., Leung, R.S., Jensen, R.E., 1997. The Tim54p–Tim22p Complex Mediates Insertion of Proteins into the Mitochondrial Inner Membrane. J. Cell Biol. 139, 1663–1675. https://doi.org/10.1083/jcb.139.7.1663

Kicka, S., Bonnet, C., Sobering, A.K., Ganesan, L.P., Silar, P., 2006. A mitotically inheritable unit containing a MAP kinase module. Proc. Natl. Acad. Sci. 103, 13445–13450. https://doi.org/10.1073/pnas.0603693103

Klanner, C., Prokisch, H., Langer, T., 2001. MAP-1 and IAP-1, two novel AAA proteases with catalytic sites on opposite membrane surfaces in mitochondrial inner membrane of Neurospora crassa. Mol. Biol. Cell 12, 2858–2869. https://doi.org/10.1091/mbc.12.9.2858

Kovermann, P., Truscott, K.N., Guiard, B., Rehling, P., Sepuri, N.B., Müller, H., Jensen, R.E., Wagner, R., Pfanner, N., 2002. Tim22, the Essential Core of the Mitochondrial Protein Insertion Complex, Forms a Voltage-Activated and Signal-Gated Channel. Mol. Cell 9, 363–373. https://doi.org/10.1016/S1097-2765(02)00446-X

Kumar, A., Scher, K., Mukherjee, M., Pardovitz-Kedmi, E., Sible, G.V., Singh, U.S., Kale, S.P., Mukherjee, P.K., Horwitz, B.A., 2010. Overlapping and distinct functions of two Trichoderma virens MAP kinases in cell-wall integrity, antagonistic properties and repression of conidiation. Biochem. Biophys. Res. Commun. 398, 765–770. https://doi.org/10.1016/j.bbrc.2010.07.020

Kurz, M., Martin, H., Rassow, J., Pfanner, N., Ryan, M.T., Craig, E.A., 1999. Biogenesis of Tim Proteins of the Mitochondrial Carrier Import Pathway: Differential Targeting Mechanisms and Crossing Over with the Main Import Pathway. Mol. Biol. Cell 10, 2461–2474. https://doi.org/10.1091/mbc.10.7.2461

Lacaze, I., Lalucque, H., Siegmund, U., Silar, P., Brun, S., 2015. Identification of NoxD/Pro41 as the homologue of the p22 ^{phox} NADPH oxidase subunit in fungi: NoxD/Pro41: the fungal p22 ^{phox} homologue. Mol. Microbiol. 95, 1006–1024. https://doi.org/10.1111/mmi.12876

Lalucque, H., Malagnac, F., Brun, S., Kicka, S., Silar, P., 2012. A Non-Mendelian MAPK-Generated Hereditary Unit Controlled by a Second MAPK Pathway in Podospora anserina. Genetics 191, 419–433. https://doi.org/10.1534/genetics.112.139469

Lamacchia, M., Dyrka, W., Breton, A., Saupe, S.J., Paoletti, M., 2016. Overlapping Podospora anserina Transcriptional Responses to Bacterial and Fungal Non Self Indicate a Multilayered Innate Immune Response. Front. Microbiol. 7. https://doi.org/10.3389/fmicb.2016.00471

Lambou, K., Malagnac, F., Barbisan, C., Tharreau, D., Lebrun, M.-H., Silar, P., 2008. The Crucial Role of the Pls1 Tetraspanin during Ascospore Germination in Podospora anserina Provides an Example of the Convergent Evolution of Morphogenetic Processes in Fungal Plant Pathogens and Saprobes. Eukaryot. Cell 7, 1809–1818. https://doi.org/10.1128/EC.00149-08

Lecellier, G., Silar, P., 1994. Rapid methods for nucleic acids extraction from Petri dish-grown mycelia. Curr. Genet. 25, 122–123. https://doi.org/10.1007/BF00309536

Liu, Y., He, C., 2016. Regulation of plant reactive oxygen species (ROS) in stress responses: learning from AtRBOHD. Plant Cell Rep. 35, 995–1007. https://doi.org/10.1007/s00299-016-1950-x

Lorin, S., Dufour, E., Boulay, J., Begel, O., Marsy, S., Sainsard-Chanet, A., 2001. Overexpression of the alternative oxidase restores senescence and fertility in a long-lived respiration-deficient mutant of Podospora anserina. Mol. Microbiol. 42, 1259–1267. https://doi.org/10.1046/j.1365-2958.2001.02690.x

Lorin, S., Dufour, E., Sainsard-Chanet, A., 2006. Mitochondrial metabolism and aging in the filamentous fungus Podospora anserina. Biochim. Biophys. Acta BBA - Bioenerg., 14th European Bioenergetics Conference 1757, 604–610. https://doi.org/10.1016/j.bbabio.2006.03.005

Macheleidt, J., Mattern, D.J., Fischer, J., Netzker, T., Weber, J., Schroeckh, V., Valiante, V., Brakhage, A.A., 2016. Regulation and Role of Fungal Secondary Metabolites. Annu. Rev. Genet. 50, 371–392. https://doi.org/10.1146/annurev-genet-120215-035203

Malagnac, F., Klapholz, B., Silar, P., 2007. PaTrx1 and PaTrx3, Two Cytosolic Thioredoxins of the Filamentous Ascomycete Podospora anserina Involved in Sexual Development and Cell Degeneration. Eukaryot. Cell 6, 2323–2331. https://doi.org/10.1128/EC.00083-07

Malagnac, F., Lalucque, H., Lepère, G., Silar, P., 2004. Two NADPH oxidase isoforms are required for sexual reproduction and ascospore germination in the filamentous fungus Podospora anserina. Fungal Genet. Biol. 41, 982–997. https://doi.org/10.1016/j.fgb.2004.07.008

Marcou, D., 1961. Notion de longévité et nature cytoplasmique du déterminant de la senescence chez quelques champignons. Ann. Sci. Nat. Bot. 653–764.

Marino, D., Dunand, C., Puppo, A., Pauly, N., 2012. A burst of plant NADPH oxidases. Trends Plant Sci. 17, 9–15. https://doi.org/10.1016/j.tplants.2011.10.001

Montero-Barrientos, M., Hermosa, R., Cardoza, R.E., Gutierrez, S., Monte, E., 2011. Functional Analysis of the Trichoderma harzianum nox1 Gene, Encoding an NADPH Oxidase, Relates Production of Reactive Oxygen Species to Specific Biocontrol Activity against Pythium ultimum. Appl. Environ. Microbiol. 77, 3009–3016. https://doi.org/10.1128/AEM.02486-10

Mukherjee, P.K., Latha, J., Hadar, R., Horwitz, B.A., 2003. TmkA, a Mitogen-Activated Protein Kinase of Trichoderma virens, Is Involved in Biocontrol Properties and Repression of Conidiation in the Dark. Eukaryot. Cell 2, 446–455. https://doi.org/10.1128/EC.2.3.446-455.2003

Munkres, K., 1990. Histochemical detection of the secretion of superoxide radicals and hydrogen peroxide by age-1 mutants of Neurospora. Fungal Genet. Rep. 37. https://doi.org/10.4148/1941-4765.1477

Osiewacz, H.D., 2011. Mitochondrial quality control in aging and lifespan control of the fungal aging model Podospora anserina. Biochem. Soc. Trans. 39, 1488–1492. https://doi.org/10.1042/BST0391488

Osiewacz, H.D., Bernhardt, D., 2013. Mitochondrial Quality Control: Impact on Aging and Life Span - A Mini-Review. Gerontology 59, 413–420. https://doi.org/10.1159/000348662

Osiewacz, H.D., Brust, D., Hamann, A., Kunstmann, B., Luce, K., Müller-Ohldach, M., Scheckhuber, C.Q., Servos, J., Strobel, I., 2010. Mitochondrial pathways governing stress resistance, life, and death in the fungal aging model Podospora anserina. Ann. N. Y. Acad. Sci. 1197, 54–66. https://doi.org/10.1111/j.1749-6632.2010.05190.x

Paoletti, M., 2016. Vegetative incompatibility in fungi: From recognition to cell death, whatever does the trick. Fungal Biol. Rev. 30, 152–162. https://doi.org/10.1016/j.fbr.2016.08.002

Pfaffl, M.W., Horgan, G.W., Dempfle, L., 2002. Relative expression software tool (REST©) for group-wise comparison and statistical analysis of relative expression results in real-time PCR. Nucleic Acids Res. 30, e36–e36. https://doi.org/10.1093/nar/30.9.e36

Razanamparany, V., Bégueret, J., 1988. Non-homologous integration of transforming vectors in the fungus Podospora anserina: sequences of junctions at the integration sites. Gene 74, 399–409. https://doi.org/10.1016/0378-1119(88)90173-4

Rizet, G., 1953a. Longevity of strains of Podospora anserina. Comptes Rendus Hebd. Seances Acad. Sci. 237, 1106–1109.

Rizet, G., 1953b. Sur l'impossibilité d'obtenir la multiplication végétative ininterrompue et illimitée de l'Ascomycète Podospora anserina. Comptes Rendus LAcadémie Sci. 838–840.

Saupe, S.J., Clavé, C., Bégueret, J., 2000. Vegetative incompatibility in filamentous fungi: Podospora and Neurospora provide some clues. Curr. Opin. Microbiol. 3, 608–612. https://doi.org/10.1016/S1369-5274(00)00148-X

Schindelin, J., Arganda-Carreras, I., Frise, E., Kaynig, V., Longair, M., Pietzsch, T., Preibisch, S., Rueden, C., Saalfeld, S., Schmid, B., Tinevez, J.-Y., White, D.J., Hartenstein, V., Eliceiri, K., Tomancak, P., Cardona, A., 2012. Fiji: an open-source platform for biological-image analysis. Nat. Methods 9, 676–682. https://doi.org/10.1038/nmeth.2019

Scott, B., 2015. Conservation of fungal and animal nicotinamide adenine dinucleotide phosphate oxidase complexes: Conservation of animal and fungal Nox. Mol. Microbiol. 95, 910–913. https://doi.org/10.1111/mmi.12946

Scott, B., Eaton, C.J., 2008. Role of reactive oxygen species in fungal cellular differentiations. Curr. Opin. Microbiol. 11, 488–493. https://doi.org/10.1016/j.mib.2008.10.008

Sellem, C.H., Marsy, S., Boivin, A., Lemaire, C., Sainsard-Chanet, A., 2007. A mutation in the gene encoding cytochrome c1 leads to a decreased ROS content and to a long-lived phenotype in the filamentous fungus Podospora anserina. Fungal Genet. Biol. 44, 648–658. https://doi.org/10.1016/j.fgb.2006.09.005

Silar, P., 2012. Hyphal Interference: Self Versus Non-self Fungal Recognition and Hyphal Death, in: Biocommunication of Fungi. Springer, Dordrecht, pp. 155–170. https://doi.org/10.1007/978-94-007-4264-2_10

Silar, P., 2005. Peroxide accumulation and cell death in filamentous fungi induced by contact with a contestant. Mycol. Res. 109, 137–149. https://doi.org/10.1017/S0953756204002230

Silar, P., 1995. Two new easy to use vectors for transformations. Fungal Genet. Rep. 42, 73. https://doi.org/10.4148/1941-4765.1353

Silar, P., Haedens, V., Rossignol, M., Lalucque, H., 1999. Propagation of a Novel Cytoplasmic, Infectious and Deleterious Determinant Is Controlled by Translational Accuracy in Podospora anserina. Genetics 151, 87–95.

Tudzynski, P., Heller, J., Siegmund, U., 2012. Reactive oxygen species generation in fungal development and pathogenesis. Curr. Opin. Microbiol. 15, 653–659. https://doi.org/10.1016/j.mib.2012.10.002

Uehling, J., Deveau, A., Paoletti, M., 2017. Do fungi have an innate immune response? An NLR-based comparison to plant and animal immune systems. PLoS Pathog. 13. https://doi.org/10.1371/journal.ppat.1006578

Vandesompele, J., De Preter, K., Pattyn, F., Poppe, B., Van Roy, N., De Paepe, A., Speleman, F., 2002. Accurate normalization of real-time quantitative RT-PCR data by geometric averaging of multiple internal control genes. Genome Biol. 3, research0034.1. https://doi.org/10.1186/gb-2002-3-7-research0034

Walker, M.A., Volpi, S., Sims, K.B., Walter, J.E., Traggiai, E., 2014. Powering the Immune System: Mitochondria in Immune Function and Deficiency. J. Immunol. Res. 2014. https://doi.org/10.1155/2014/164309

Weil, A., Luce, K., Dröse, S., Wittig, I., Brandt, U., Osiewacz, H.D., 2011. Unmasking a temperature-dependent effect of the P. anserina i-AAA protease on aging and development. Cell Cycle Georget. Tex 10, 4280–4290. https://doi.org/10.4161/cc.10.24.18560

West, A.P., Shadel, G.S., Ghosh, S., 2011. Mitochondria in innate immune responses. Nat. Rev. Immunol. 11, 389–402. https://doi.org/10.1038/nri2975

Wichmann, G., Sun, J., Dementhon, K., Glass, N.L., Lindow, S.E., 2008. A novel gene, phcA from Pseudomonas syringae induces programmed cell death in the filamentous fungus Neurospora crassa. Mol. Microbiol. 68, 672–689. https://doi.org/10.1111/j.1365-2958.2008.06175.x

Tables:

Table 1: strains and genotypes

genotype	*Detailed genotype*	resistance markers	reference
wild type	*big S*	-	(Rizet, 1953b)
Δmus51	*Δmus51::su8-1*	-	(Lambou et al., 2008)
Δmus51	*Δmus51::phleoR*	phleoR	(El-Khoury et al., 2008)
mito-GFP	*mito-GFP::hygR*	hygR	(Sellem et al., 2007)
ΔPaMpk1	*ΔPaMpk1::hygR*	hygR	(Kicka et al., 2006)
PaNox1^{-}	*IDC*^{343}	-	(Malagnac et al., 2004)
ΔPaTrx2	*ΔPaTrx2::phleoR*	phleoR	(Malagnac et al., 2007)
PaTim54^{2218}	*PDC*^{2218}	-	(Haedens et al., 2005)
			This study
ΔPaCdk5	*ΔPaCdk5::hygR*	hygR	
ΔPaNip30	*ΔPaNip30::nouR*	nouR	
*ΔPaTim54**	*ΔPaTim54::hygR*	hygR	
ΔPaCdk5 ΔPaNip30		hygR nouR	
ΔPaCdk5 pPaCdk5 pBC-phleo		hygR phleoR	
ΔPaCdk5 ΔPaNip30 pPaCdk5 pBC-phleo		hygR phleoR nouR	
mat+/mat- ΔPaTim54/+		hygR	
ΔPaTim54 pBC-phleo-PaTim54		hygR phleoR	
PaTim54^{2218} *ΔPaMpk1*		hygR	
PaTim54^{2218} *PaNox1*$^{-}$		-	
PaTim54^{2218} *pPaCdk5 pBC-phleo*		phleoR	
PaTim54^{2218} *pBC-hyg-Cdk5*		hygR	
PaTim54^{2218} *PaCdk5*^{PCR} *pBC-hyg*		hygR	
PaTim54^{2218} *pBC-hyg-PaTim54*		hygR	
PaTim54^{2218} *pBC-phleo-PaTim54*		phleoR	
PaTim54^{2218} *PaTim54*^{PCR} *pBC-hyg*		hygR	
PaTim54^{2218} *mito-GFP*		hygR	
PaTim54^{2218} *pBC-phleo-PaTim54 mito-GFP*		phleoR hygR	

*: homokaryotic lethal

Table 2: *PaTim54^{2218} pBC-hyg-PaCdk5 X WT*

PaTim54^{2218} pBC-hyg-PaCdk5 X WT	phenotypes			
	[WT hygR]	[WT hygS]	[PaTim54^{2218} hygS]	Genetic linkage : χ^2 test
2	21	15	0	Yes: d<2.7cM : P<10^{-2}
3	21	27	0	Yes: d<2.0cM : P<10^{-9}
4	22	23	0	Yes: d<2.1cM : P<10^{-4}
transformant number	*PaTim54^{2218}, pBC-hyg-PaCdk5*	*+,+*	*PaTim54^{2218}, +*	
	genotypes			

Table 3: *ΔPaCdk5 pPaCdk5 pBC-phleo X WT*

ΔPaCdk5 {pPaCdk5 pBC phleo} X	phenotypes			
WT	[hygR phleoR]	[hygS phleoS]	[hygS phleoR]	[hygR phleoS]
2	6 [WT]	15 [WT]	9 [WT]	12 [ΔPaCdk5]
6	9 [WT]	12 [WT]	10 [WT]	13 [ΔPaCdk5]
7	11 [WT]	14 [WT]	10 [WT]	13 [ΔPaCdk5]
transformant number	*ΔPaCdk5, pPaCdk5 pBC-phleo*	*+, +*	*+, pPaCdk5 pBC-phleo*	*ΔPaCdk5, +*
	genotypes			

Table 4: *ΔPaCdk5 pPaCdk5 pBC-phleo X PaTim54^{2218}*

ΔPaCdk5 {pPaCdk5 pBC phleo} X	phenotypes			
PaTim54^{2218}	[hygR phleoR]	[hygS phleoS]	[hygS phleoR]	[hygR phleoS]
2 (F1)	7 [WT]	9 [PaTim54^{2218}]	7 [PaTim54^{2218}]	17 [ΔPaCdk5]
6 (F1)	9 [WT]	16 [PaTim54^{2218}]	8 [PaTim54^{2218}]	10 [ΔPaCdk5]
7 (F1)	11 [WT]	8 [PaTim54^{2218}]	11 [PaTim54^{2218}]	4 [ΔPaCdk5]
transformant number	*ΔPaCdk5, pPaCdk5 pBC-phleo*	*PaTim54^{2218}, +*	*PaTim54^{2218}, pPaCdk5 pBC-phleo*	*ΔPaCdk5, +*
	genotypes			

Table 5: *PaTim54^{2218} pBC-hyg-PaTim54 X WT*

PaTim54^{2218} pBC-hyg-PaTim54 X WT	phenotypes			
	[WT hygR]	[WT hygS]	[PaTim54^{2218} hygS]	Genetic linkage χ^2
3	17	12	3	no : p>0.05
4	18	8	5	no : p >0.05
5	22	12	5	no : p >0.05
transformant number	*PaTim54^{2218}, pBC-hyg-PaTim54 or +, pBC-hyg-PaTim54*	*+,+*	*PaTim54^{2218}, +*	
	genotypes			

Table 6: tetrad analysis of *mat+/mat- ΔPaTim54/+ X WT mat–* or *mat+*

ΔPaTim54/+ X *WT*	crossing with *mat -*			crossing with *mat +*		
	phenotype	genotype	number	phenotype	genotype	number
FDS asci	2 [†]	*ΔPaTim54/ΔPaTim54*	3			
	2 [hygS]	*+/+*		4 [hygS]	+/+	8
SDS asci	4 [hygR]	*ΔPaTim54/+*	7			

Table 7: *mat- PaTim54^{2218} pBC-phleo-PaTim54 X mat+/mat- ΔPaTim54/+*

mat- PaTim54^{2218} pBC-phleo-PaTim54 X mat+/mat- ΔPaTim54/ +	phenotypes			
	[hygS phleoR]	[hygR phleoS]	[hygR phleoR]	[hygS phleoS]
	21 [WT]	0	4 [WT]	8 [PaTim54^{2218}]
	PaTim54^{2218}, pBC-phleo-PaTim54	*ΔPaTim54, +*	*ΔPaTim54, pBC-phleo-PaTim54*	*PaTim54^{2218}, +*
	genotypes			

Figures captions:

Figure 1: Phenotypes of the different strains and Hyphal Interference assays (HI). A) vegetative growth of the different strains on standard M2 medium (first column); DAB staining (second column); Evans Blue staining (third column). Scale bars: 1 cm. **B)** schematic of the Hyphal Interference assay: The *P. anserina* tested strains are co-inoculated with three *Penicillium chrysogenum* (*P. c*) *inocula*. The oxidative burst as well as cell death revealed by DAB staining (brownish patch) and Evans blue staining (blue crescent) respectively are performed after 3 days on different plates incubated in parallel. **C)** results of the HI assays for the different genotypes tested. EB: Evans blue; DAB: diaminobenzidin; semi-quantitative staining scoring -: no significant staining; +, ++, +++: staining of increasing intensity.

Figure 2: Growth rate on M2 standard medium. A) Growth rate at 27°C, the standard temperature. *WT*: 6.6 ± 0.5 mm/day; *PaTim54^{2218}* (*PDC^{2218}*)*: 5.5* ± 0,5 mm/day; *PaTim54^{2218} pBC-phleo-PaTim54* : 6.4 ± 0.3 mm/day. *: n=18; t-test P<10^{-6}; * for *PaTim54^{2218}* is the t-test probability in comparison with *WT*. **B)** relative growth rate of *PaTim54^{2218}* and *PaTim54^{2218} pBC-phleo-PaTim54* strains at different temperatures. No growth for *PaTim54^{2218}* at 37°C. The result at 27°C is from the experiment in A). * for *PaTim54^{2218}* is the t-test probability in comparison with *WT*. Relative growth rate values for *PaTim54^{2218} pBC-phleo-PaTim54* are never significantly different to *WT.*

Figure 3: Chromosome map of the *PaTim54^{2218}* (*PDC^{2218}*) locus. Upper part, diagram of the whole chromosome 6 (K6). Both polymorphic markers *214-1*, *yeti1*, the *PaTrx2* gene and the mutation *PDC^{2218}* renamed *PaTim54^{2218}* (*) are reported and the distances are indicated in kbp. The regions covered by both 11G02 and 31C04 cosmids are indicated. Lower part, map of the *PaTim54^{2218}* locus.

The CDS of the three investigated genes *PaCdk5 (Pa_6_9000)*, *PaNip30* (*Pa_6_9010*) and *PaTim54* (*Pa_6_9020*) are represented. The 1560 pb deletion identified in the *PaTim54*^{2218} mutant is indicated by the corresponding dashed line. This deletion removes the first 140 bp of *PaNip30* CDS. The region covered by the *PaCdk5* ESTs is indicated by the corresponding dashed line. The wild-type genomic DNA fragments which have been used for complementation experiments, and encompassing *PaCdk5, PaNip30* or *PaTim54* CDSs are represented. Sizes of the CDSs upstream sequences are indicated as negative starting from the start codon and size of CDSs downstream sequences are indicated as positive starting from the stop codon. bp: base pairs.

Figure 4: *PaCdk5, PaTim54 and PaAOX genes* expression level. Expression analysis by RT-qPCR of *PaCdk5* (*Pa_ 6_9000*), *PaTim54* (*Pa_ 6_9020*) and *PaAOX* (*Pa_3_1710*) in strains of interest. Genotypes are indicated on the vertical axis. Horizontal axis indicates the decimal logarithm of fold change (FC) in transcript detection relative to the wild-type strain (see Table S6 and S7 for Cq and Table S8 for numerical values of FC). Normalization genes selected with geNorm (Vandesompele et al., 2002) were *AS1*, *GPD* and *UBC*, with an average stability value M= 0.346 and $V_{3/4}$ = 0.093 (see Table S6). Bars show standard errors and stars (*) indicate FC with a p-value < 0.05 (see Table S8 for numerical values of standard errors). FCs with a 95 % confidence interval including the ratio 1 or very close to 1 were not considered as significant, even if the p-value is below the cut-off (du Prel et al., 2009).

Figure 5: Mitochondria and nucleoids in *PaTim54*^{2218}. A) Epifluorescence microscopy photographs of strains carrying the mito-GFP reporter. In these strains, the Green Fluorescent Protein is imported into mitochondria and visualized in the green channel. Genotypes: *WT :+, mito-GFP*; *PaTim54*^{2218} :*PaTim54*^{2218}*, mito-GFP* and *PaTim54*^{2218} *pBC-phleo-PaTim54 : PaTim54*^{2218} *pBC-phleo-PaTim54 mito-GFP*. DAPI stains nucleoids (mtDNA) and is visualized in the blue channel. Scale bar: 5 µm. **B)** DAPI

tagged nucleoids have been counted in 10 µm-long hyphal segments (n=20) for every genotypes**. C)** and **D)** The size (diameter) of 20 nucleoids (n=20) and the diameter of 20 mitochondria (n=20) have been determined on two to five representative fields of view (pictures) depending on the genotype analyzed (see Mat & Met). T-test P values are indicated in each panel.

Figure 6: Mitochondria of *P. anserina* during HI. Z series photographs of hyphae of *P. anserina* (*P. a*) and *Penicillium chrysogenum* (*P. c*) in confrontation. The mitochondrial network is highlighted by the *mito-GFP* reporter gene present in both the control *mito-GFP* and the *PaTim54*^{2218} *mito-GFP* strains. First column, DIC; second column, GFP fluorescence. Arrow heads indicate budding branching hyphae specifically observed in *PaTim54*^{2218} but not in the control. Scale bar= 10µm.

Figure 7: mtDNA level quantification and senDNA analysis. A) Copy number analysis by qPCR of *NAD4* in strains of interest. Genotypes are indicated on the vertical axis. Horizontal axis indicates fold change (FC) in copy number detection relative to the wild-type strain (see Table S9 for Cq and Table S10 for numerical values of FC). Three nuclear loci were used for normalization (Table S9). Bars show standard errors and stars (*) indicate FC with a p-value < 0.05 (see Table S5 for numerical values of standard errors). **B) Senescent DNA (senDNA) analysis.** DNA was digested by *H*aeIII and stained with Ethidium Bromide. Two DNA sample replicates (1 and 2) -used for the mtDNA level quantification- per genotype were analyzed. MW, Molecular Weight marker. Bands sizes are indicated in base pairs (bp). Wt_{sen}, genomic DNA extracted from senescent *WT* strain. * Senescent DNA. Senescent DNA was not detected in the DNA samples used for the qPCR-based mtDNA quantification experiment.

Figure 8: Longevity assay. Total growth distance after 191 days incubation for triplicate cultures of three individual freshly germinated homokaryotic ascospores of both mating types for each analyzed genotype. In grey, dead cultures before day 191; in black, alive and still growing cultures at day 191. Every dead cultures eventually presented senescence on their thallus. (*): P values <0.05 for the t-tests performed between the *PaTim54*^{2218} strain and the *WT* ($P<4.10^{-8}$) or the *PaTim54*^{2218} *pBC-phleo-PaTim54* complemented strain ($P<4.10^{-8}$).

Figures:

Figure 1:

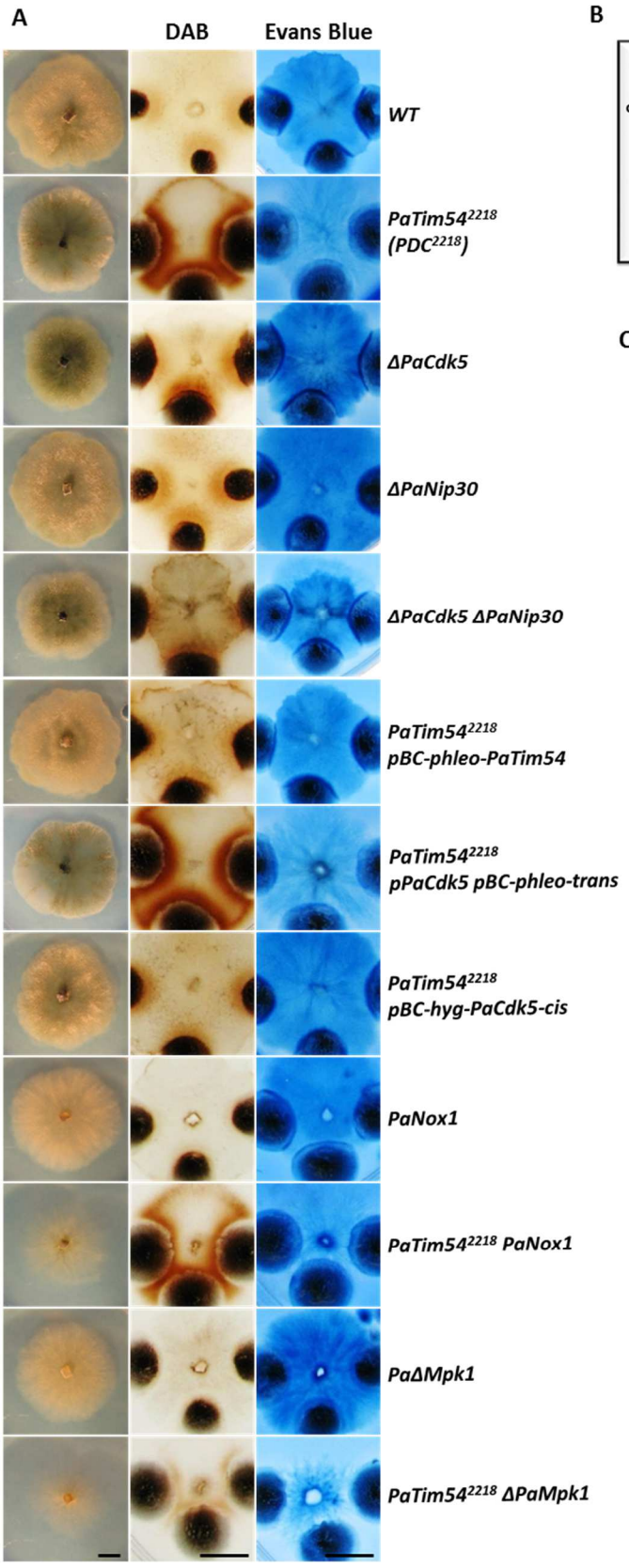

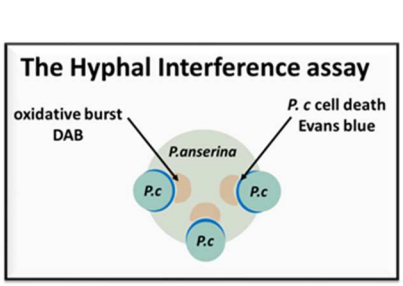

C

genotypes	DAB	EB
WT	+	+
PaTim54^2218 (PDC^2218)	+++	-
Δ PaCdk5	+	+
ΔPaNip30	+	+
ΔPaCdk5 ΔPaNip30	+	+
PaTim54^2218 pBC-hyg-PaTim54	+	+
PaTim54^2218 pBC-hyg-PaCdk5-trans	+++	-
PaTim54^2218 pBC-hyg-PaCdk5-cis	+	+
PaNox1	-	-
PaTim54^2218 PaNox1	+++	-
PaΔMpk1	-	-
PaTim54^2218 ΔPaMpk1	+	-

Figure 2:

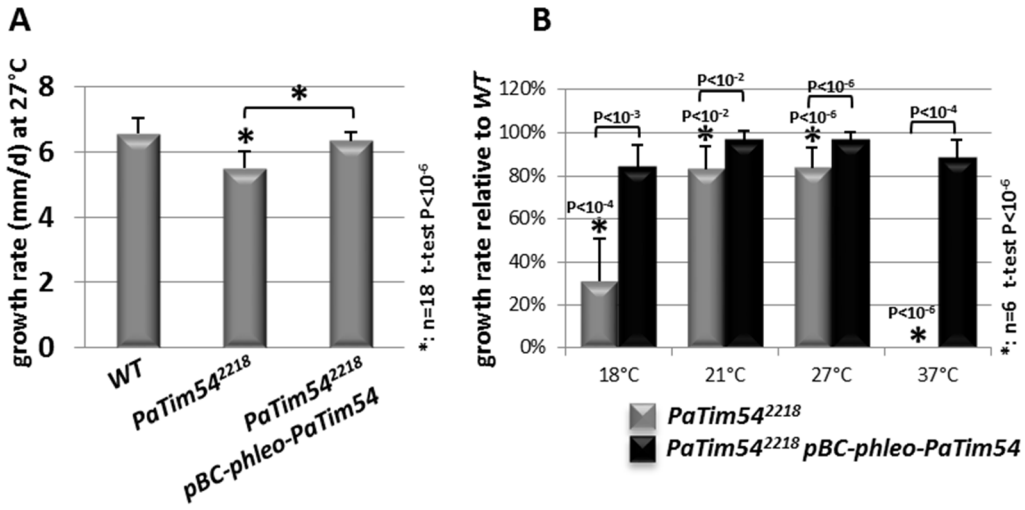

Figure 3:

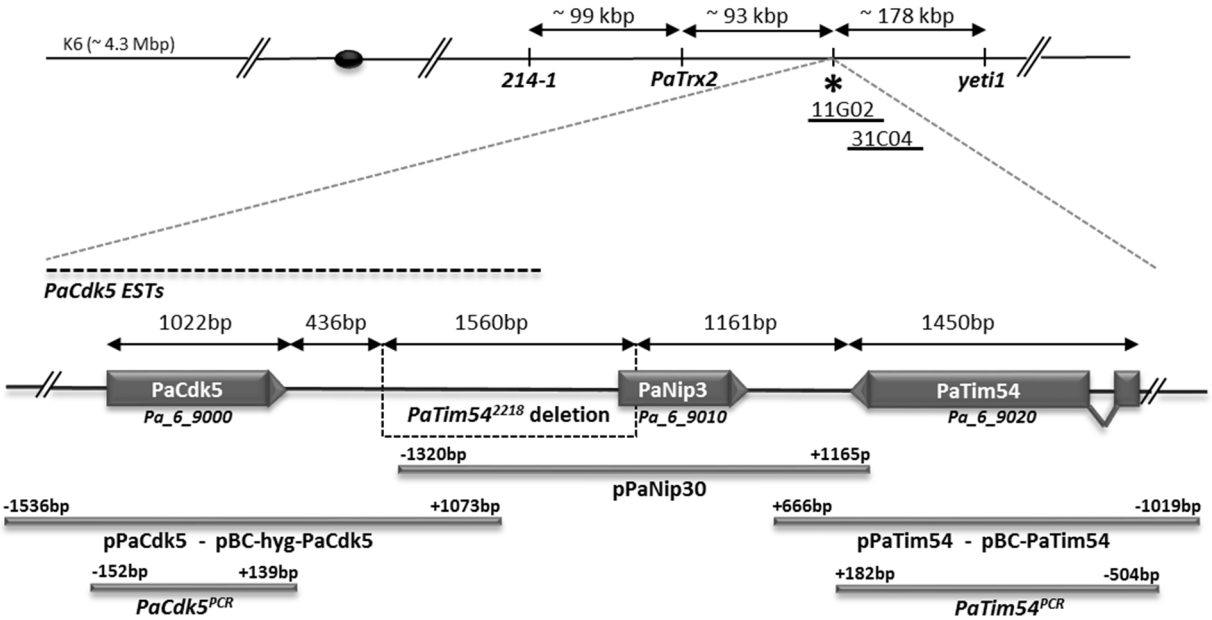

Figure 4:

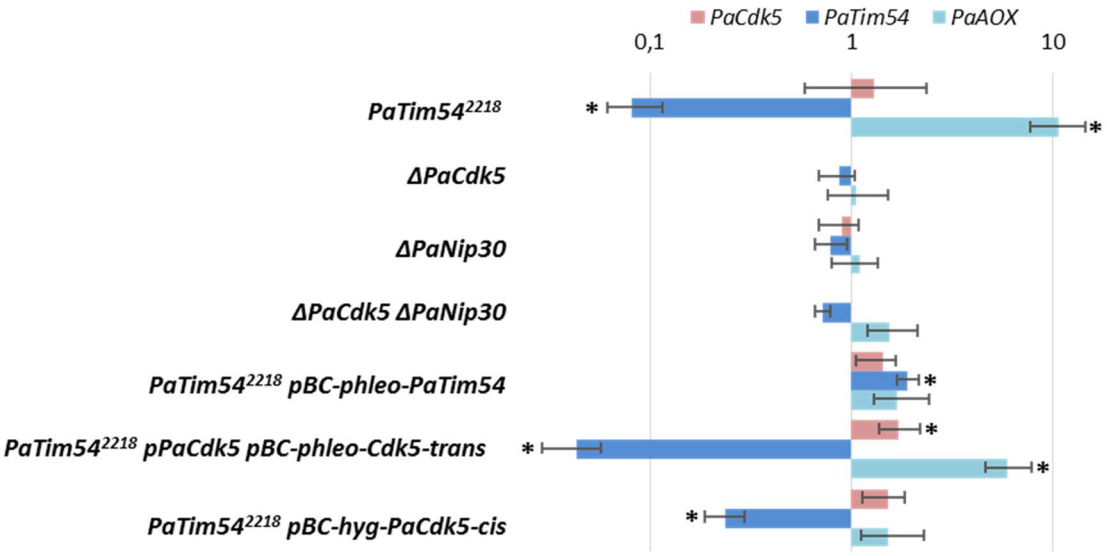
PaCdk5
PaTim54
PaAOX
0,1
1
10
PaTim54^2218
ΔPaCdk5
ΔPaNip30
ΔPaCdk5 ΔPaNip30
PaTim54^2218 pBC-phleo-PaTim54
PaTim54^2218 pPaCdk5 pBC-phleo-Cdk5-trans
PaTim54^2218 pBC-hyg-PaCdk5-cis

Figure 5:

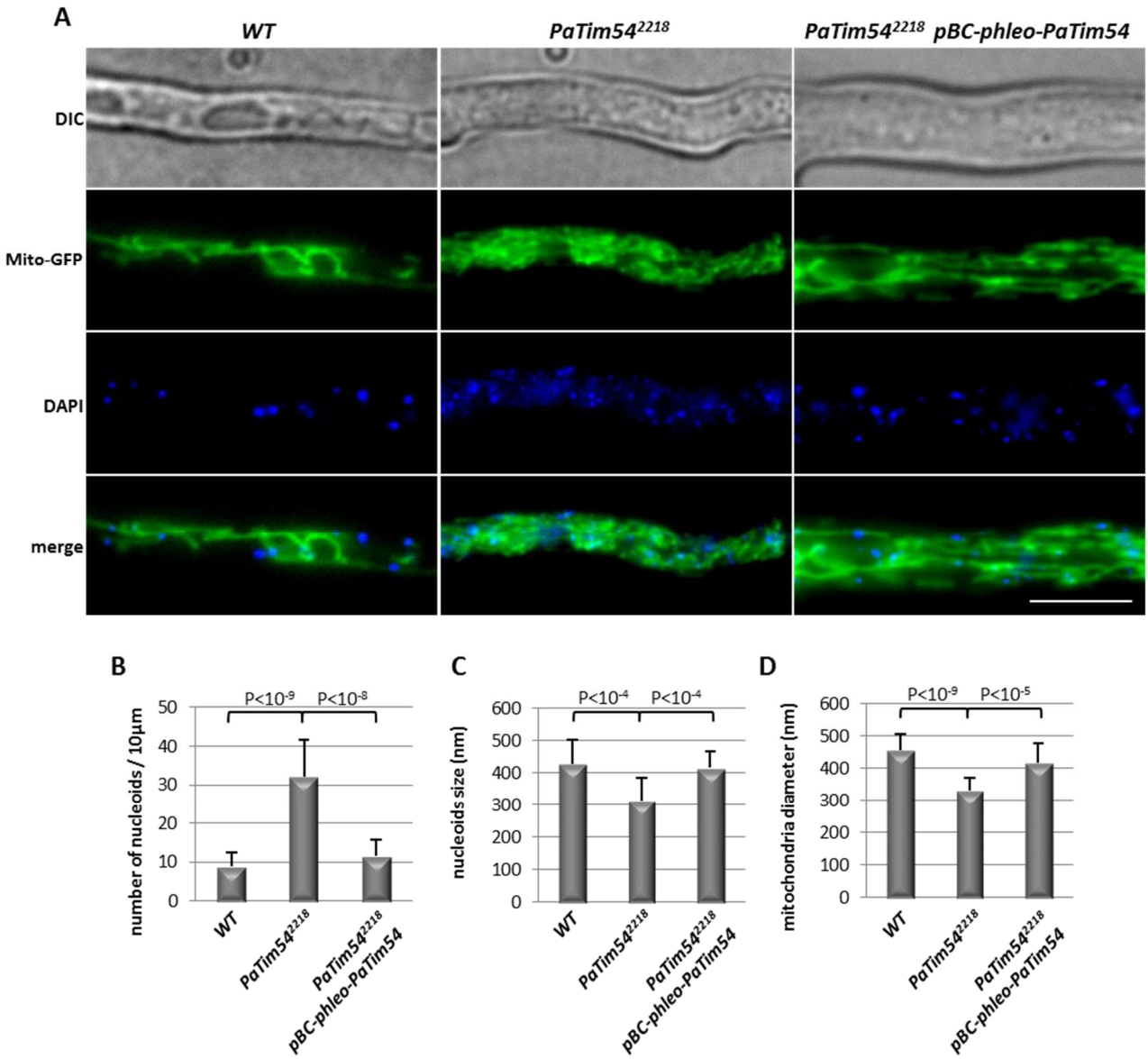
A
WT
PaTim54^2218
PaTim54^2218 pBC-phleo-PaTim54
DIC
Mito-GFP
DAPI
merge
B
number of nucleoids / 10µm
P<10-9
P<10-8
C
nucleoids size (nm)
P<10-4
P<10-4
D
mitochondria diameter (nm)
P<10-9
P<10-5
WT
PaTim54^2218
PaTim54^2218 pBC-phleo-PaTim54

Figure 6:

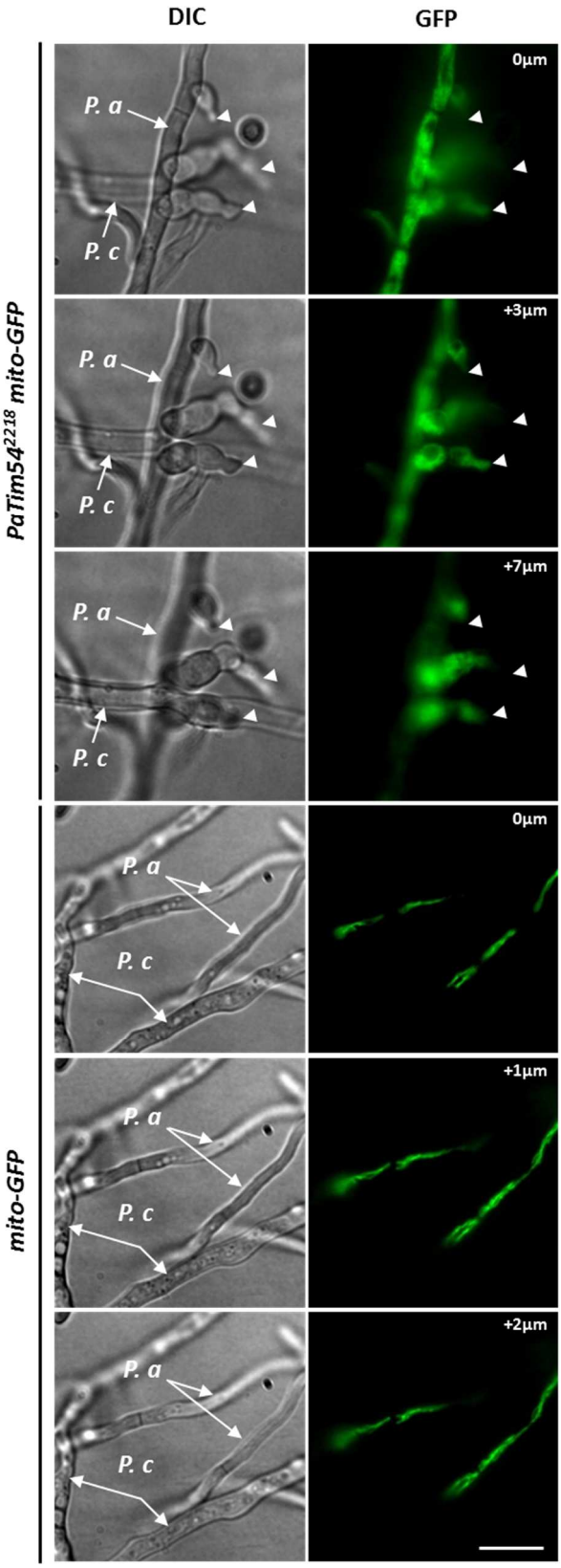

1150

Figure 7:

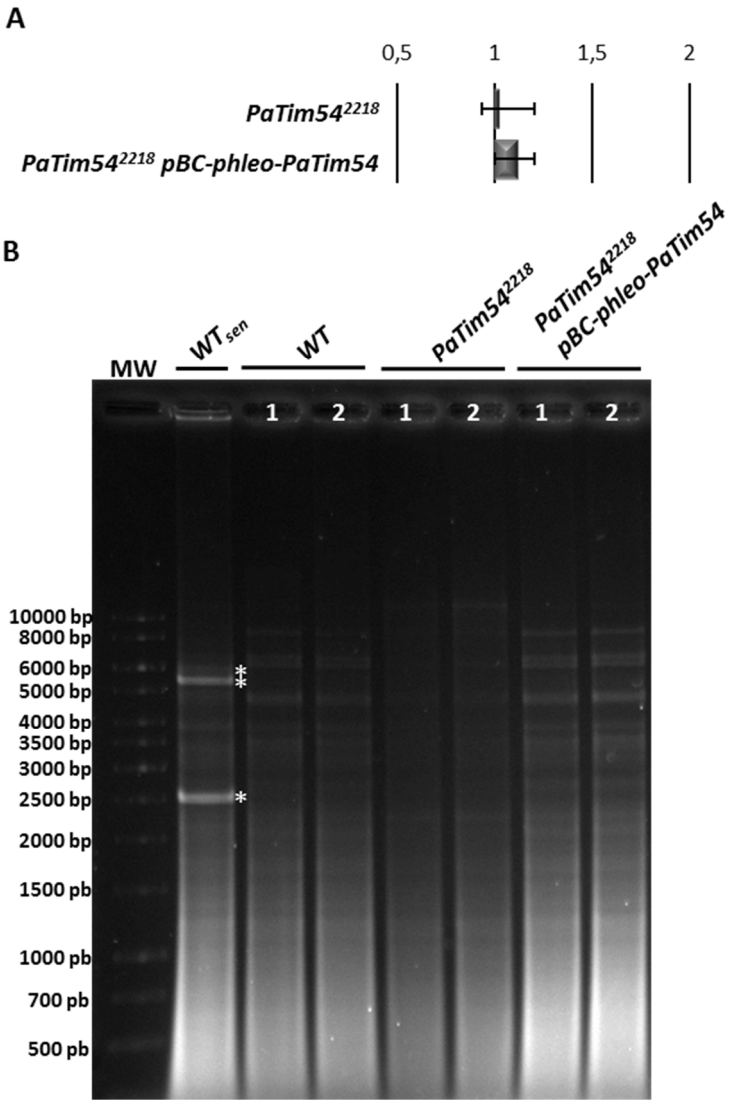
A
0,5
1
1,5
2
PaTim54^{2218}
PaTim54^{2218} pBC-phleo-PaTim54
B
MW
WT$_{sen}$
WT
PaTim54^{2218}
PaTim54^{2218} pBC-phleo-PaTim54
1
2
1
2
1
2
10000 bp
8000 bp
6000 bp
5000 bp
4000 bp
3500 bp
3000 bp
2500 bp
2000 bp
1500 pb
1000 pb
700 pb
500 pb

Figure 8:

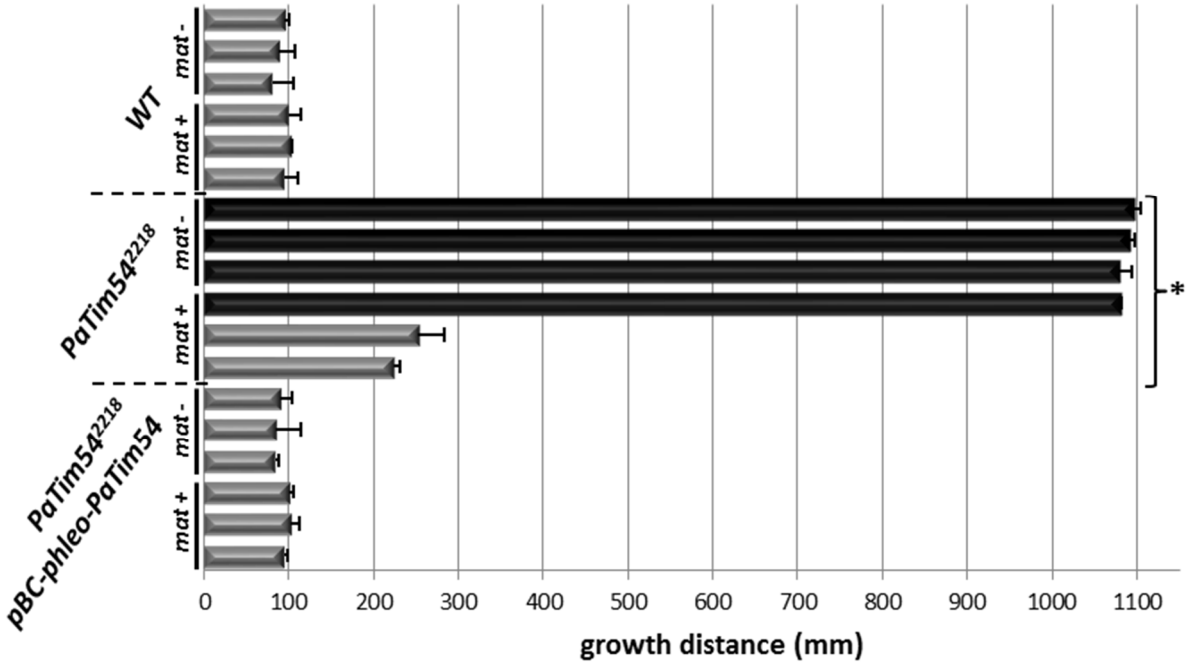

1151

Supplemental Informations:

Table S1_S5 : genetics analyses data and primers tables.

Table_S6. Cq for the housekeeping genes and identification of the normalization genes with geNorm [1]. Cq for *PaTim54* (Pa_6_9020).

Table_S7. Cq for *AS1* (Pa_1_16650), *GPD* (Pa_3_5110), *UBC* (Pa_4_7790), *PaAOX* (Pa_3_1710) and *PaCdk5* (Pa_6_9000).

Table_S8. Fold changes and standard errors for *PaCdk5* (Pa_ 6_9000), *PaTim54* (Pa_ 6_9020) and *PaAOX* (Pa_3_1710).

Table_S9. Cq for the quantification of mitochondrial DNA.

Table_S10. Fold changes and standard errors for mitochondrial DNA quantification.

Figure S1: *ΔPaCdk5, ΔPaNip30, ΔPaCdk5 ΔPaNip30 ΔPaTim54 and deletions.*

Figure S2: Protein sequence alignment of PaTim54 from *P. anserina*, NcTim54 from *N. crassa* and ScTim54 from *Saccharomyces cerevisiae*.

Figure S3: Measures of Green Fluorescence maximum intensities in hyphae of the *mito-GFP* control strain and of the *PaTim54*^{2218} *mito-GFP* strain.

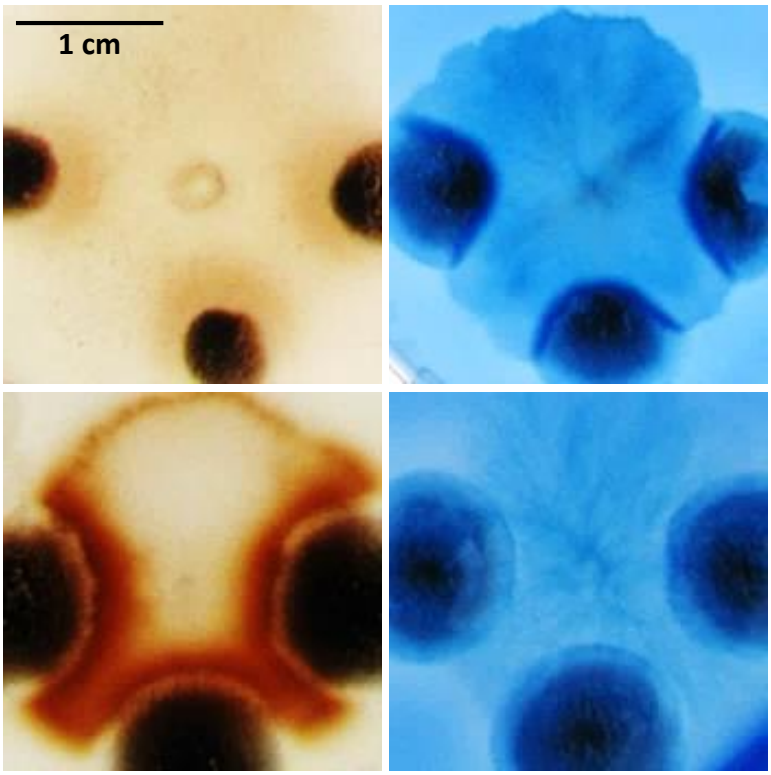
1 cm